

 Open access • Posted Content • DOI:10.1101/639070

Group B rotavirus encodes a functional fusion-associated small transmembrane (FAST) protein — [Source link](#)

Julia R. Diller, Helen M. Parrington, John T. Patton, Kristen M. Ogden





Institutions: Vanderbilt University Medical Center, National Institutes of Health

Published on: 15 May 2019 - bioRxiv (Cold Spring Harbor Laboratory)

Topics: NSP1, Rotavirus, Tropism and Reoviridae

Related papers:

- [Rotavirus Species B Encodes a Functional Fusion-Associated Small Transmembrane Protein.](#)
- [In vivo interactions among rotavirus nonstructural proteins](#)
- [Two-amino acids change in the nsp4 of SARS coronavirus abolishes viral replication.](#)
- [Structural Analysis of Porcine Reproductive and Respiratory Syndrome Virus Non-structural Protein 7 \$\alpha\$ \(NSP7 \$\alpha\$ \) and Identification of Its Interaction with NSP9.](#)
- [II, 7. Interaction of the rotavirus nonstructural glycoprotein NSP4 with viral and cellular components](#)

Share this paper:    

View more about this paper here: <https://typeset.io/papers/group-b-rotavirus-encodes-a-functional-fusion-associated-1gk9pes2w3>

1 **Group B rotavirus encodes a functional fusion-associated small**
2 **transmembrane (FAST) protein**

3

4 Julia R. Diller^a, Helen M. Parrington^b, John T. Patton^{c†}, and Kristen M. Ogden^{a,b#}

5

6 Department of Pediatrics, Vanderbilt University Medical Center, Nashville, Tennessee,

7 USA^a; Department of Pathology, Microbiology, and Immunology, Vanderbilt University

8 Medical Center, Nashville, Tennessee, USA^b; Laboratory of Infectious Diseases,

9 National Institute of Allergy and Infectious Diseases, National Institutes of Health,

10 Bethesda, Maryland, USA^c

11

12 Running head: Group B rotavirus encodes a FAST protein

13

14 #Address correspondence to Kristen M. Ogden, kristen.ogden@vumc.org

15

16 †Present address: John Patton, Department of Biology, Indiana University,

17 Bloomington, Indiana, USA

18

19 Abstract word count: 243

20 Text word count: 6,601

21

22 **ABSTRACT**

23 Rotavirus is an important cause of diarrheal disease in young mammals. Group A
24 rotavirus (RVA) causes most human rotavirus diarrheal disease and primarily affects
25 infants and young children. Group B rotavirus (RVB) has been associated with sporadic
26 outbreaks of human adult diarrheal disease. RVA and RVB are predicted to encode
27 mostly homologous proteins but differ significantly in the proteins encoded by the NSP1
28 gene. In the case of RVB, the NSP1 gene encodes two putative protein products of
29 unknown function, NSP1-1 and NSP1-2. We demonstrate that human RVB NSP1-1
30 mediates syncytia formation in cultured human cells. Based on sequence alignment,
31 NSP1-1 from groups B, G, and I contain features consistent with fusion-associated
32 small transmembrane (FAST) proteins, which have previously been identified in other
33 *Reoviridae* viruses. Like some other FAST proteins, RVB NSP1-1 is predicted to have
34 an N-terminal myristoyl modification. Addition of an N-terminal FLAG peptide disrupts
35 NSP1-1-mediated fusion, consistent with a role for this fatty-acid modification in NSP1-1
36 function. NSP1-1 from a human RVB mediates fusion of human cells but not hamster
37 cells and, thus, may serve as a species tropism determinant. NSP1-1 also can enhance
38 RVA replication in human cells, both in single-cycle infection studies and during a multi-
39 cycle time course in the presence of fetal bovine serum, which inhibits rotavirus spread.
40 These findings suggest potential yet untested roles for NSP1-1 in RVB species tropism,
41 immune evasion, and pathogenesis.

42

43 **IMPORTANCE**

44 While group A rotavirus is commonly associated with diarrheal disease in young
45 children, group B rotavirus has caused sporadic outbreaks of adult diarrheal disease. A
46 major genetic difference between group A and B rotaviruses is the NSP1 gene, which
47 encodes two proteins for group B rotavirus. We demonstrate that the smaller of these
48 proteins, NSP1-1, can mediate fusion of cultured human cells. Comparison with viral
49 proteins of similar function provides insight into NSP1-1 domain organization and fusion
50 mechanism. Our findings are consistent with an important role for a fatty acid
51 modification at the amino terminus of the protein in mediating its function. NSP1-1 from
52 a human virus mediates fusion of human cells, but not hamster cells, and enhances
53 rotavirus replication in culture. These findings suggest potential, but currently untested,
54 roles for NSP1-1 in RVB species tropism, immune evasion, and pathogenesis.

55 INTRODUCTION

56 Rotaviruses are members of the *Reoviridae* family of nonenveloped viruses with
57 segmented dsRNA genomes and causative agents of diarrheal disease in many young
58 mammals, including humans. Adults are often resistant to rotavirus diarrheal disease.
59 Acquired immunity, particularly local and systemic antibodies, plays an important role in
60 protection from rotavirus disease, and immunity appears to increase with repeated
61 infection or immunization (1). However, innate immunity also may contribute to rotavirus
62 disease, and rotaviruses have been shown to antagonize innate signaling pathways
63 using multiple distinct mechanisms (1-3).

64 Rotaviruses are currently classified into eight species, A-I, which further resolve
65 into two major clades (<https://talk.ictvonline.org/>) (4-6). One clade contains species A,
66 C, D, and F, and the other contains species B, G, H, and I. The majority of human
67 rotavirus diarrheal disease occurs in infants and young children and is associated with
68 rotavirus species A (RVA) (1). RVA also causes diarrheal disease in birds and
69 numerous mammals, though subsets of RVA genotypes are associated with specific
70 hosts (7). RVB, RVC, RVH, and RVI have been detected mostly in domesticated
71 mammals, while RVD, RVF, and RVG have been detected in birds. However, instances
72 of zoonotic transmission of rotaviruses and their gene segments, particularly between
73 humans and domesticated animals, have been documented (8, 9). Although some
74 factors, such as lack of appropriate attachment and entry machinery or adaptive
75 immune cross-protection, are known to impose barriers, factors permitting or limiting
76 rotavirus zoonotic transmission remain incompletely understood.

77 Evidence of RVB infection has been commonly detected in diarrheic pigs (10-12),
78 and RVB has been associated with sporadic outbreaks of diarrheal disease in humans
79 (13-16). The first reported human RVB outbreak occurred in China from 1982-1983,
80 ultimately affecting more than a million people with cholera-like diarrhea (17-21). While
81 RVB disease symptoms resemble those of RVA gastroenteritis, RVB causes disease
82 primarily in adults rather than pediatric populations (22). Studies suggest there is low-
83 level RVB seroprevalence in humans (23-25). RVB outbreaks in humans are not
84 thought to be caused by viruses directly transmitted from animals; rather, phylogenetic
85 analysis of RVB sequences suggests viruses affecting humans and other animals are
86 distinct (26). Factors contributing to the capacity of these viruses to cause disease in
87 adults remain unknown.

88 Like RVA, RVB have genomes containing 11 segments of dsRNA. Based on
89 sequence alignment and structure prediction, 10 of the 11 RVB segments encode
90 proteins with RVA homologs (27, 28). However, the segment encoding RVA innate
91 immune antagonist NSP1 differs significantly. For most rotaviruses in the clade
92 containing RVB, including RVG and RVI, the NSP1 gene segment contains two
93 overlapping ORFs whose encoded protein products have little predicted sequence or
94 structural homology with known proteins (29). The first RVB ORF, NSP1-1, is predicted
95 to encode a product approximately 100 amino acids in length (Fig. 1A), though the
96 protein product has not been shown to be expressed. The length and predicted
97 structural features of NSP1-1 are reminiscent of fusion-associated small
98 transmembrane (FAST) proteins.

99 FAST proteins are a family of small, bitopic plasma membrane proteins that
100 mediate cell-cell fusion and syncytium formation (reviewed in (30, 31)). These
101 nonstructural viral proteins are encoded by fusogenic members of the *Aquareovirus* and
102 *Orthoreovirus* genera of the nonenveloped *Reoviridae* virus family. There are multiple
103 types of FAST proteins, and they range in size from approximately 90-200 amino acids.
104 Each contains three modular domains: a small, N-terminal extracellular domain that is
105 often acylated, a transmembrane domain, and a C-terminal cytoplasmic tail containing a
106 polybasic motif. Additional putative functional motifs have been identified and vary
107 among FAST protein family members. FAST proteins are nonstructural proteins that are
108 expressed following virus entry, viral mRNA transcription, and translation. Membrane
109 fusion occurs in closely apposed cells. FAST protein clustering and interactions with the
110 opposing lipid bilayer, including insertion of fatty acid moieties or hydrophobic residues,
111 favors lipid mixing and membrane curvature, leading to pore formation. Following pore
112 formation, cellular proteins, including annexin 1 and actin promote pore expansion and,
113 thereby, syncytia formation.

114 In the current publication, we provide evidence that RVB NSP1-1 is a FAST
115 protein that is capable of mediating syncytia formation in some, but not all, mammalian
116 cell types. Based on sequence alignment, we suggest that other rotavirus species, RVG
117 and RVI, also may encode functional FAST proteins. We demonstrate that the N
118 terminus is required for NSP1-1-mediated fusion and provide experimental support for a
119 role of NSP1-1 in viral replication and spread. These findings have potential implications
120 for the role of NSP1-1 in host immune evasion and human RVB disease.

121

122 **RESULTS**

123 **The N terminus is required for RVB NSP1-1-mediated fusion in 293T cells.** To test
124 the hypothesis that NSP1-1 is a FAST protein, we transfected human embryonic kidney
125 293T cells with a pCAGGS vector, pCAGGS encoding the fusogenic Nelson Bay
126 orthoreovirus (NBV) p10 FAST protein (32), or pCAGGS encoding codon-optimized
127 human RVB Bang117 NSP1-1, permitted expression for 24 h, then examined cell
128 morphology using differential interference contrast microscopy. Transfection with NBV
129 p10, a known FAST protein (32-35), or with RVB NSP1-1 changed the cell morphology
130 from individually distinct cells to a monolayer pockmarked by smooth oval-shaped
131 regions lacking defined cell edges, which likely represent syncytia (Fig. 1B). These
132 observations suggest that, like NBV p10, RVB NSP1-1 can mediate cell-cell fusion.

133 To enable detection of RVB NSP1-1, we engineered a FLAG peptide at the N or
134 C terminus. Following transfection of 293T cells with pCAGGS encoding tagged forms
135 of RVB NSP1-1, we found that C-terminally tagged NSP1-1 (NSP1-1-FLAG) mediated
136 morphological changes resembling syncytia in the cell monolayer (Fig. 1B). Cells
137 transfected with plasmids encoding N-terminally tagged NSP1-1 (FLAG-NSP1-1),
138 however, were morphologically indistinguishable from vector-transfected cells. This
139 finding suggests that the N terminus plays an important role in RVB NSP1-1-mediated
140 cell morphological changes.

141 To gain insight into RVB NSP1-1 localization and cell morphological changes, we
142 transfected 293T cells with pCAGGS encoding FLAG tagged NSP1-1, waited 24 h to
143 permit protein expression, fixed and stained the cells to detect FLAG and nuclei, and
144 imaged them using confocal microscopy. FLAG-NSP1-1 was typically expressed in the

145 cytoplasm of individual, or sometimes adjacent, cells (Fig. 2A). In Z-stacks, FLAG-
146 NSP1-1 was detected in the cytoplasm at the level of the nucleus, and individual stained
147 cells were distinct (Fig. 2C). In striking contrast to FLAG-NSP1-1, NSP1-1-FLAG was
148 detected in clusters containing many nuclei (Fig. 2B). When looking through a Z-stack,
149 NSP1-1-FLAG was detected at and above the level of the nucleus, consistent with
150 cellular and plasma membrane localization, and the edges of individual stained cells
151 were indistinguishable (Fig. 2D).

152

153 **Shared features of RVB NSP1-1 and *Reoviridae* FAST proteins.** The similarity in
154 protein size and cell morphological changes induced upon RVB NSP1-1 expression
155 suggested that it may be a FAST protein. To gain insight into the relationships between
156 rotavirus NSP1-1 proteins and *Reoviridae* FAST proteins, we constructed a maximum
157 likelihood (ML) tree using the sequences of representative RVB, RVG, and RVI NSP1-1
158 proteins and orthoreovirus and aquareovirus FAST proteins (Fig. 3A). We found that
159 aquareovirus, and ARV/NBV FAST proteins each formed a clade supported by strong
160 bootstrap values that clustered distinctly from the rotavirus NSP1-1 proteins and BRV
161 p15, BroV p13, and RRV p14 FAST proteins. While they did not cluster together
162 strongly, RVB and RVG NSP1-1 proteins clustered most closely with BRV p15, whereas
163 RVI NSP1-1 proteins clustered more closely with RRV p14.

164 To gain insight into sequence and structural features of rotavirus NSP1-1
165 proteins, we used software to scan for sequence motifs and constructed amino acid
166 alignments with the most closely clustering FAST proteins from the ML tree (Fig. 3A).
167 Based on the PROSITE definition (PDOC00008), an N-myristoylation site was predicted

168 at amino acids 2-7 in RVB NSP1-1 (Fig. 3B). Although there is a high false-positive
169 prediction rate for N-myristoylation motifs, prediction at this precise location for every
170 complete RVB, RVG, and RVI NSP1-1 sequence deposited in GenBank (as of
171 12/4/2018; Fig. S1) provides confidence in its legitimacy. BroV, RRV, and BRV FAST
172 proteins are also known or predicted to be N-myristoylated (36-39). Using the TMHMM
173 Server, we identified predicted transmembrane helices in RVB, RVG, and RVI
174 sequences (Fig. 3B). In each case, the N terminus was predicted to be extracellular,
175 while the C terminus was predicted to be cytoplasmic. For RVB Bang117 NSP1-1, the
176 TM region was predicted to span amino acids 39-61. The N termini of the NSP1-1
177 proteins in the alignment were typically predicted to be shorter than those of the FAST
178 proteins. Like the BroV, RRV, and BRV FAST proteins, each of the NSP1-1 proteins
179 contained multiple basic residues shortly after the TM domain (Fig. 3B). However, fewer
180 basic residues were present in NSP1-1 (4-5) than FAST (6-7) protein polybasic regions.
181 Some RVB sequences contain short stretches of hydrophobic residues in the N-terminal
182 domain, while others contain two short hydrophobic regions in the C-terminal domain
183 (Fig. 3B). Analyzed RVG and RVI NSP1-1 proteins lacked strong hydrophobic
184 signatures outside of the predicted transmembrane domain. NSP1-1 proteins were
185 typically shorter than FAST proteins, by up to 36 amino acids, with most of the
186 difference in length residing C terminal to the polybasic region (Fig. 3B). The motifs
187 identified by sequence alignment and analysis (Fig. 3B) suggest models of RVB NSP1-
188 1 in which the extracellular, myristoylated N-terminal domain precedes a single
189 transmembrane domain and a short cytoplasmic tail containing a polybasic region, with
190 some RVB NSP1 proteins containing a single hydrophobic region N-terminal to the

191 transmembrane domain and others containing two hydrophobic regions C-terminal to
192 the polybasic region (Fig. 3C).

193

194 **RVB NSP1-1 mediates syncytia formation in Caco-2 cells.** Rotaviruses infect
195 enterocytes in the human intestine. To determine whether RVB Bang117 NSP1-1 could
196 mediate syncytia formation in a more biologically relevant cell type, we transfected
197 human epithelial colorectal adenocarcinoma Caco-2 cells with pCAGGS encoding
198 FLAG-tagged RVB NSP1-1. These cells can form polarized monolayers and
199 morphologically and functionally resemble the enterocytes lining the small intestine. To
200 achieve reasonable transfection efficiency, we transfected subconfluent Caco-2
201 monolayers, waited 24 or 48 h to permit protein expression, fixed and stained the cells
202 to detect FLAG and nuclei, then imaged them using indirect immunofluorescence
203 microscopy. Similar to observations made in 293T cells (Fig. 2A), we found that FLAG-
204 NSP1-1 was primarily expressed in the cytoplasm of individual Caco-2 cells or small
205 numbers of adjacent cells, whereas NSP1-1-FLAG was expressed mostly in the
206 cytoplasm of clusters of cells containing multiple nuclei and lacking distinct cell
207 boundaries (Fig. 4A). We quantified the numbers of single cells and clusters (at least
208 three immediately adjacent FLAG-positive cells) present in wells of transfected Caco-2
209 cells at 24 h post transfection. Consistent with a role for the N terminus in cell-cell
210 fusion, we found that there were significantly more FLAG-positive single cells in FLAG-
211 NSP1-1-transfected than NSP1-1-FLAG-transfected wells (~9 fold) and significantly
212 more clusters present in NSP1-1-FLAG-transfected cells than FLAG-NSP1-1-
213 transfected wells (~3.5 fold) (Fig. 4B). Often, groups of FLAG-NSP1-1-transfected cells

214 we identified as “clusters” appeared to be groups of three or four adjacent singly
215 transfected cells. To quantify differences in cluster size between FLAG-NSP1-1-
216 transfected and NSP1-1-transfected Caco-2, we measured cluster diameters and found
217 that diameters of NSP1-1-FLAG clusters were significantly larger than those of FLAG-
218 NSP1-1 (Fig. 4C). These findings suggest that C-terminally tagged RVB Bang117
219 NSP1-1 can mediate fusion of a cell type similar to that targeted during natural RVB
220 infection.

221
222 **RVB NSP1-1 fails to mediate fusion in BHK cells.** We next wanted to test RVB
223 NSP1-1 function in the context of viral infection. NBV p10 enhances reovirus and
224 rotavirus replication in baby hamster kidney cells expressing T7 RNA polymerase (BHK-
225 T7 cells) (32). The reverse genetics system for simian rotavirus strain SA11 involves
226 transfection of BHK-T7 cells with plasmids encoding the 11 rotavirus RNAs under the
227 control of the T7 promoter, along with pCAGGS plasmids encoding viral capping
228 enzymes, to enhance viral protein translation, and NBV p10, to enhance rotavirus
229 replication and spread. We hypothesized that, if RVB NSP1-1 could mediate syncytia
230 formation in BHK-T7 cells, it could functionally replace NBV p10 in rotavirus reverse
231 genetics experiments. As a first step towards this goal, we transfected BHK-T7 cells
232 with pCAGGS alone or pCAGGS expressing NBV p10, FLAG-NSP1-1, or NSP1-1-
233 FLAG, waited 24 h to permit protein expression, fixed and stained the cells to detect
234 FLAG and nuclei, and imaged them using differential interference contrast and indirect
235 immunofluorescence microscopy. Transfection with pCAGGS encoding NBV p10
236 resulted in the appearance of balls or ring-like clusters of nuclei surrounded by regions

237 of smooth cytoplasm nearly devoid of nuclei (Fig. 5B). Although many transfected cells
238 detectably expressed NSP1-1-FLAG or FLAG-NSP1-1, no morphological differences
239 were detected in comparison to vector-transfected cells, and all cells had distinct
240 borders (Fig. 5A,C-D). A similar lack of morphological change was observed following
241 transfection of BHK-T7 cells with untagged RVB NSP1-1 (not shown). Although
242 localization was not examined in depth, NSP1-1-FLAG staining did not often diffusely fill
243 the cytoplasm but appeared as perinuclear puncta, suggesting potential mislocalization
244 (Fig. 5D). These findings suggest that RVB NSP1-1 is incapable of mediating cell-cell
245 fusion in all mammalian cell lines.

246

247 **RVB NSP1-1 mediates enhanced RVA replication in human cells.** Since NSP1-1 did
248 not mediate cell-cell fusion in BHK-T7 cells, we sought to test RVB NSP1-1 function in
249 the context of viral infection in Caco-2 and 293T cells, which can support RVA
250 replication and RVB NSP1-1-mediated fusion. Although the precise mechanism is
251 unknown, NBV p10 has been shown to enhance replication of simian RVA strain SA11
252 in cells adsorbed at low multiplicity of infection (MOI) during a 16 h time course, which is
253 less than the time required to complete a round of replication and initiate infection of a
254 new subset of cells (32). Trypsin, which cleaves viral attachment protein VP4, activates
255 RVA for optimal infectivity (1). To determine whether NBV p10 or RBV NSP1-1 affected
256 viral replication in Caco-2 or 293T cells, we transfected these cells with increasing
257 concentrations of pCAGGS alone or pCAGGS encoding NBV p10 or RVB NSP1-1, then
258 infected them with trypsin-activated RVA strain SA11. At 16 h post infection, we lysed
259 the cells and quantified viral titers. We found that SA11 titer was enhanced in Caco-2

260 cells transfected with 2 μ g of NBV P10 or 1 or 2 μ g of NSP1-1, in comparison to vector-
261 transfected cells (Fig. 6A). A very modest but statistically significant enhancement of
262 SA11 titer also was detected in 293T cells transfected with 2 or 10 ng of pCAGGS
263 expressing RVB NSP1-1, in comparison to vector-transfected cells (Fig. 6B). These
264 findings suggest a potential role for RVB NSP1-1 in enhancing rotavirus replication in
265 human cells during a single infectious cycle.

266 Rotavirus spreads poorly in cultured cells in the presence of fetal bovine serum
267 (FBS), likely due to inhibited cleavage of the viral attachment protein. To determine
268 whether RVB NSP1-1 could facilitate rotavirus spread in the presence of FBS, we
269 transfected Caco-2 or 293T cells with pCAGGS alone or pCAGGS encoding NBV p10
270 or RVB NSP1-1, then infected them with RVA strain SA11 and incubated them in
271 standard culture medium containing 20% FBS (Caco-2) or 10% FBS (293T). At 24 h
272 and 48 h post transfection, we lysed the cells and quantified viral titer. In Caco-2 cells,
273 we found a modest increase in SA11 titer (<10-fold) at 24 h post infection in RVB NSP1-
274 1 transfected cells in comparison to vector-transfected cells (Fig. 6C). No significant
275 difference in titer was detected at 48 h post infection. However, by this time, RVB
276 NSP1-1-transfected Caco-2 monolayers displayed evidence of significant cytopathic
277 effects, including cell rounding and lifting, which may indicate poor cell health (Fig. 6E).
278 In 293T cells, we found that SA11 titers were significantly enhanced for both NBV p10-
279 and RVB NSP1-1-transfected cells, in comparison to vector-transfected cells at 24 and
280 48 h post infection (Fig. 6D). Transfection of 293T cells with similar amounts of
281 pCAGGS expressing RVB NSP1-1 results in modest (24 h) to significant (48 h) visible
282 syncytium formation within the monolayer, without complete monolayer disruption and

283 cell lifting (Fig. 6E). Together, these findings suggest that RVB NSP1-1 can enhance
284 rotavirus replication during multi-cycle infection, perhaps by enabling cell-cell spread.

285

286 **DISCUSSION**

287 Based on our findings, we propose that RVB encode functional FAST proteins
288 that contain a myristoyl moiety on the N terminus, an extracellular N-terminal loop, a
289 central transmembrane helix, and a relatively short cytoplasmic tail containing a region
290 of approximately four basic residues (Fig. 3C). Short stretches of hydrophobic residues
291 also are predicted in either the N- or C-terminal regions of the protein. The
292 morphological changes induced in cultured cells following NSP1-1 expression, which
293 include the appearance of smooth patches lacking distinct cell membranes and
294 resemble those induced by NBV p10, suggest that RVB NSP1-1 can mediate syncytia
295 formation in human 293T cells (Fig. 1B). The detection of FLAG-positive multinucleated
296 clusters in NSP1-1-FLAG transfected 293T and Caco-2 cells suggests that the cells
297 expressing NSP1-1 are fusing to one another, and addition of a peptide to the C
298 terminus does not disrupt fusion activity (Figs. 2 and 4). The reduced number of clusters
299 in FLAG-NSP1-1-transfected 293T and Caco-2 cells suggests that the N terminus plays
300 an important role in fusion and is consistent with disruption of the N-terminal myristoyl
301 moiety (Figs. 2-4). While the proposed sequence and structural features of RVB NSP1-
302 1 remain to be biochemically and structurally validated, sequence alignment and
303 analysis support our model of RVB NSP1-1 organization (Fig. 3). For example, the
304 presence of a predicted myristoylation motif at the N terminus of every RVB, RVG, and

305 RVI sequence in GenBank (Figs. 3B and S1) provides support for the presence of this
306 fatty acid modification.

307 If our model is correct, RVB NSP1-1 proteins are the shortest and simplest
308 proteins shown to mediate functional cell-cell fusion. Conservation of a fatty acid
309 modification at the N terminus and the polybasic motif in the cytoplasmic tail in all
310 NSP1-1 proteins, as well as clusters of hydrophobic residues in either the N- or C-
311 terminal domain, suggests these motifs may be critical for protein function (Figs. 3B-C
312 and S1). The myristoylated N terminus and hydrophobic patch residues of FAST
313 proteins induce lipid mixing between liposomal membranes (37, 40). While insertion of
314 N-terminal fatty acid and hydrophobic moieties may promote membrane merger,
315 cytoplasmic hydrophobic patches may promote pore formation by partitioning into the
316 curved rim of a newly formed fusion pore (31). Sequence alignments suggest that RVG
317 and RVI also may encode FAST proteins (Fig. 3B), though their functionality remains to
318 be tested. It will be informative to determine whether these proteins can mediate cell-
319 cell fusion in the absence of evident hydrophobic patches and polyproline motifs. If
320 functional, RVI NSP1-1 will represent the smallest known FAST protein and may help
321 define the minimal requirements for cell-cell fusion. Expansion of the repertoire of
322 known viral FAST proteins may enable the establishment of guidelines that permit
323 identification of additional novel viral FAST proteins, despite their highly divergent
324 sequences.

325 Many viruses exhibit tropism for certain animal species or cell types. Zoonotic
326 transmission, however, is a frequent but often incompletely understood phenomenon.
327 Virus and host factors can serve as barriers to transmission or virulence factors

328 following zoonotic transmission. Based on the observation that it can mediate fusion in
329 human cells but not hamster cells, NSP1-1 may serve as a viral tropism determinant.
330 However, cells from many different animal species and tissue types, as well as NSP1-1
331 proteins from rotaviruses derived from different animal hosts, will need to be tested
332 before the boundaries of this limitation are revealed. Support for the idea that there are
333 host species preferences comes from the observation that NSP1 gene sequences of
334 RVBs from murine, human, ovine, bovine, and porcine hosts cluster in distinct
335 phylogenetic groups, with low identities between them and the greatest diversity
336 detected among porcine RVBs (26). Why NBV p10 FAST is capable of mediating fusion
337 in BHK-T7 cells, while RVB NSP1-1 is not, currently is unclear. While RVB NSP1-1 is
338 predicted to be myristoylated at the N terminus, p10 FAST proteins form an extracellular
339 cysteine loop and are not myristoylated but are palmitoylated at a membrane-proximal
340 site in the N terminus (34, 41-43). These differences in acylation may affect
341 functionality. Based on apparent mislocalization of NSP1-1, it is possible that signals
342 that mediate trafficking from the endoplasmic reticulum, where FAST proteins are
343 translated, to the plasma membrane, via the secretory pathway (38, 44-47), fail to
344 function appropriately in some non-homologous hosts. Chimeric FAST proteins
345 containing individual domain exchanges between RVB Bang117 NSP1-1 and NBV p10,
346 similar to those engineered by Eileen Clancy for other FAST proteins (30, 31, 48), may
347 provide insight into protein domains responsible for the species-specific fusion activity of
348 RVB Bang117 NSP1-1.

349 Expression of NSP1-1 during infection has not been shown. A direct attempt to
350 detect expression of a product from the NSP1-1 ORF following *in vitro* transcription and

351 translation from full-length IDIR gene 7 and immunoprecipitation with convalescent rat
352 serum proved unsuccessful (29). In the same publication, the authors predicted efficient
353 NSP1-2 translation and much less efficient NSP1-1 translation based on nucleotide
354 sequences flanking the START codons (29). However, villous epithelial syncytial cell
355 formation has been observed in the ileum and jejunum of RVB IDIR-infected neonatal
356 rats, with syncytial cells reported to contain large numbers of viral particles (49, 50).
357 Additionally, an ovine RVB strain produced RVB-positive syncytia on MA104
358 monolayers (51). In numerous studies of RVB in pigs and cows, researchers have failed
359 to note detection of syncytia, though they may not have been looking for such events.
360 However, in a rodent model of infection with a fusogenic pteropine orthoreovirus (PRV),
361 authors failed to detect syncytia in infected lung tissue when specifically looking for
362 these cells (33). In the case of RVB infection, it has been suggested that syncytia are
363 rapidly sloughed from the intestinal epithelium and therefore easily missed (51). These
364 observations suggest that NSP1-1 is expressed during RVB infection, but low levels of
365 expression and cytotoxic effects may render this protein, and the syncytia whose
366 formation it mediates, difficult to detect.

367 Our results with cells transiently transfected with plasmids expressing RVB
368 NSP1-1 and infected with RVA SA11 suggest potential functions for NSP1-1 in rotavirus
369 replication and spread (Fig. 6). Since only a single successful *in vitro* culture system has
370 been published for RVB (52), with no follow-up studies, we used RVA to study NSP1-1
371 function in the context of viral infection. Our experimental results support a role for RVB
372 NSP1-1 in enhancing rotavirus replication in the presence of trypsin at a time point less
373 than the length of a single infectious cycle (Fig. 6A-B) and in the presence of inhibitory

374 FBS at time points that would permit multiple rounds of replication (Fig. 6C-D). The
375 latter result is consistent with enhancement of replication by permitting the virus to
376 spread from cell-to-cell without having to initiate infection at the plasma membrane,
377 whereas the former result suggests another mechanism of replication enhancement. A
378 major drawback to our experiments using RVA is the inability to ensure that NSP1-1
379 expression and viral infection occurred in the same cell. With a small percentage of cells
380 infected and only a subset of cells transfected with plasmid DNA, it is likely that only a
381 fraction of infected cells also fused to adjacent cells to mediate virus spread. In our
382 system, we also were unable to modulate NSP1-1 expression levels, and our codon-
383 optimized expression construct may have yielded significantly higher levels of protein
384 expression than are likely to occur during natural infection, fusing cells too rapidly and
385 resulting in cell death (Fig. 6E). Ultimately, these preliminary observations will need to
386 be validated in a more biologically relevant system. Our results are consistent with
387 those from other published studies showing that FAST proteins can enhance replication
388 of dsRNA viruses on sub-single-cycle and multi-cycle time scales (32, 33). In one study,
389 the authors detected enhancement of viral RNA synthesis in the presence of FAST
390 proteins as early as five hours post infection, and they hypothesized that cell-to-cell
391 fusion provides access to additional substrates for viral transcription, such as nucleotide
392 triphosphates and S-adenosyl methionine (33). Since replication enhancement
393 conferred by FAST proteins was detected even at high MOI, the authors suggested that
394 enhancement is not mediated by cell-to-cell spread. Mechanisms by which cell fusion
395 could enhance viral replication at high MOI remain unclear, as fusion would not be

396 anticipated to provide access to new sources of material for building progeny virions
397 under these conditions.

398 What is the biological function of RVB NSP1-1 during infection? Syncytia formed
399 between epithelial cells may increase rates of cell-to-cell spread and enhancing viral
400 replication and shedding within the infected host. This hypothesis is supported by the
401 previous detection of syncytial cells, which were reported to contain the majority of virus
402 particles, at the tips of jejunal and ileal villi during RVB infection of neonatal rats (49,
403 50). Close cellular apposition, mediated by adherens junctions, facilitates FAST protein-
404 mediated fusion (53). Thus enterocytes, which form close contacts via tight junctions,
405 are ideal candidate cells for FAST protein-mediated syncytium formation. While the
406 hypothesis remains to be tested, our findings (Fig. 6C-D) suggest the possibility that
407 cell-to-cell fusion induced by NSP1-1 aids in the spread of RVB strains following
408 introduction into the gastrointestinal tract. Such a mechanism could potentially enable
409 immune evasion within the host by permitting viral spread in the presence of
410 neutralizing antibodies. A report of dairy cows involved in a 2002 RVB diarrhea outbreak
411 shedding a highly similar strain of RVB during a 2005 outbreak suggests that animals
412 are not completely protected after the initial infection (54), though RVA reinfection with
413 reduced disease severity also occurs (1, 55). Regardless of mechanism, there is now
414 published evidence supporting a biological role for a FAST protein *in vivo* (33). In a
415 rodent model, two PRV viruses that are isogenic except in the capacity to express p10
416 FAST exhibited significant differences in pathogenesis, with animals infected with PRV
417 containing an intact FAST protein exhibiting reduced body weight and survival and
418 enhanced viral titer and lung pathology, in comparison to animals infected with PRV

419 lacking p10 FAST expression. While we currently lack a system in which to directly test
420 its function, these observations suggest a potential role for RVB NSP1-1 and other
421 FAST proteins in viral replication and pathogenesis *in vivo*.

422 Although it is reasonable to anticipate that NSP1-1 permits evasion of adaptive
423 immune responses by promoting direct rotavirus cell-to-cell spread within the host, it is
424 unclear how RVB and other viruses in its clade (RVG, RVH, and RVI) evade innate
425 immune signaling in the absence of an RVA NSP1 homolog. RVA NSP1 has been
426 shown to promote degradation of innate signaling molecules, including interferon
427 regulatory factors and β -TrCP (3, 56). In some cases, RVA NSP1 function is host
428 species-specific. Perhaps cell-cell fusion permits rotavirus to evade some innate
429 immune mechanisms, or perhaps NSP1-2, whose function remains unknown, obviates
430 the need for an RVA-like NSP1 protein. The evolutionary mechanisms through which
431 FAST proteins became incorporated into rotavirus genomes, or *Reoviridae* genomes in
432 general, and consequences of the lack of an NSP1-1 ORF for RVH viruses also are
433 unclear (57). Future studies using new animal models and technologies, such as
434 reverse genetics and human intestinal organoid culture (32, 58), may permit insights
435 into differences in host interactions among the rotavirus species.

436

437 **MATERIALS AND METHODS**

438 **Cells, viruses, and antibodies.** Human embryonic kidney 293T cells were
439 grown in Dulbecco's modified Eagle's minimal essential medium (Corning)
440 supplemented to contain 10% fetal bovine serum (FBS) (Gibco) and 2 mM L-glutamine.
441 Human colonic epithelial Caco-2 cells were grown in Eagle's minimum essential

442 medium (MEM) with Earle's salts and L-glutamine (Corning) supplemented to contain
443 20% FBS, 1X MEM non-essential amino acids (Sigma), 10 mM HEPES (Corning), and
444 1 mM sodium pyruvate (Gibco). Monkey kidney epithelial MA104 cells were grown in
445 MEM with Earle's salts and L-glutamine (Corning) supplemented to contain 5% FBS.
446 Baby hamster kidney cells expressing T7 RNA polymerase under control of a
447 cytomegalovirus promoter (BHK-T7) (59) were grown in Dulbecco's modified Eagle's
448 minimal essential medium (Corning) supplemented to contain 5% fetal bovine serum, 2
449 mM L-glutamine, and 10% tryptose phosphate broth (Gibco). These cells were
450 propagated in the presence of 1 mg/ml G418 (Invitrogen) during alternate passages.

451 Simian rotavirus laboratory strain SA11 was propagated in MA104 cells, and viral
452 titers were determined by FFA using MA104 cells (60).

453 Monoclonal mouse anti-FLAG antibody (Sigma), sheep polyclonal rotavirus
454 antiserum (Invitrogen), Alexa Fluor 546-conjugated anti-mouse IgG (Invitrogen), and
455 Alexa Fluor 488-conjugated anti-sheep IgG (Invitrogen) are commercially available.

456 **Plasmids.** NBV p10 in pCAGGS has been described previously (32). pLIC8 was
457 constructed by engineering a ligation-independent cloning site in mammalian
458 expression plasmid pGL4.74. pLIC6 was constructed by engineering a ligation-
459 independent cloning site into mammalian expression plasmid pCAGGS. RVB Bang117
460 was sequenced from a specimen obtained in 2002 from a 32 year-old male with severe
461 diarrhea in Bangladesh (61). A codon-optimized version of RVB Bang117 NSP1-1 was
462 synthesized (Genscript) and cloned into pLIC8 and pLIC6 using ligation-independent
463 cloning following PCR amplification with appropriate primers and T4 DNA polymerase
464 treatment. Tagged versions of NSP1-1 were engineered using 'round the horn PCR.

465 Briefly, a pair of primers, each encoding half of the FLAG peptide (DYKDDDDK), was
466 used to amplify NSP1-1 in pLIC8. Then, the PCR fragment was purified and ligated to
467 form a complete tag inserted at the N or C terminus of the ORF. After verifying the
468 sequences of plasmid clones, tagged versions of NSP1-1 were transferred into pLIC6
469 using ligation-independent cloning, and nucleotide sequences were verified by Sanger
470 sequencing.

471 **Cell Transfection and Imaging.** For differential interference contrast imaging,
472 293T cells ($\sim 5 \times 10^5$ per well) in 12-well plates were transfected with 0.2 μg of plasmid
473 DNA per well using LyoVec transfection reagent (InvivoGen), according to manufacturer
474 instructions, incubated at 37°C for 24 h, and imaged using a Zeiss Axiovert 200 inverted
475 microscope. For confocal imaging, glass coverslips were sterilized, coated with poly-L-
476 lysine (Sigma), rinsed, and dried. 293T cells (1.25×10^5 per well) were seeded onto
477 coverslips in 24-well plates and incubated at 37°C one day prior to transfection with 0.1
478 μg of plasmid DNA per well using LyoVec. At 24 h post transfection, cells were fixed
479 with cold methanol and blocked with PBS containing 1% FBS. FLAG peptides were
480 detected with mouse anti-FLAG diluted 1:500, and Alexa Fluor 546-conjugated anti-
481 mouse IgG, diluted 1:1000, and nuclei were detected using 300 nM 4',6-diamidino-2-
482 phenylindole (DAPI, Invitrogen), with washes in PBS containing 0.5% Triton X-100
483 (Fisher Scientific). Stained coverslips were mounted on glass slides using ProLong Gold
484 antifade mountant (Invitrogen) and dried prior to imaging with an Olympus FV-1000
485 Inverted confocal microscope.

486 BHK-T7 cells ($\sim 2 \times 10^5$ per well) in 24-well plates were transfected with 0.5 μg of
487 plasmid DNA per well using TransIT-LT1 transfection reagent (Mirus Bio) in OptiMEM

488 (Gibco), according to manufacturer instructions, and incubated at 37°C for 24 h prior to
489 fixing and staining. Cells were fixed with cold methanol and blocked with PBS
490 containing 1% FBS. Staining to detect FLAG and nuclei was performed as described
491 above. Stained cells were imaged using a Zeiss Axiovert 200 inverted microscope
492 equipped with an HBO 100 mercury arc lamp.

493 Caco-2 cells ($\sim 1 \times 10^5$ per well) in 24-well plates were transfected with 1 μ g per
494 well of plasmid DNA using TransIT-LT1 transfection reagent in OptiMEM, according to
495 manufacturer instructions, and incubated at 37°C for 24 h prior to fixing and staining.
496 Cells were fixed with 10% neutral buffered formalin and blocked with PBS containing
497 0.5% Triton X-100 and 5% FBS. Staining to detect FLAG and nuclei was performed as
498 described above. Stained cells were imaged using a Zeiss Axiovert 200 inverted
499 microscope equipped with an HBO 100 mercury arc lamp.

500 **Quantitation of single cells, clusters, and cluster diameter.** Caco-2 cells in
501 24-well plates were transfected with 1 μ g per well of plasmids encoding RVB Bang117
502 NSP1-1-FLAG or RVB Bang117 FLAG-NSP1-1 and stained to detect FLAG and nuclei
503 as described for imaging studies. Clusters were defined as groupings of at least three
504 FLAG-positive cells in contact with one another. To quantify single cells and clusters,
505 entire wells of transfected cells were visually analyzed using a Zeiss Axiovert 200
506 inverted microscope. The person analyzing the wells was not the person who performed
507 the transfections and in most cases was blinded to the identity of the samples. Four
508 independent experiments each containing three technical replicates were analyzed. To
509 quantify cluster diameter, entire wells of transfected cells from the four independent
510 experiments just described were imaged using an ImageXpress Micro XL automated

511 microscope imager (Molecular Devices). Diameters of 20 cell clusters per plasmid
512 construct per experiment were quantified using MetaXpress image analysis software
513 v6.5 (Molecular Devices). To compare numbers of clusters, single cells, and cluster
514 diameters, statistical analyses were performed using unpaired t-tests with GraphPad
515 Prism 7 (GraphPad).

516 **Transfection-Infection Experiments in Caco-2 cells.** For short-term rotavirus
517 transfection-infection experiments, Caco-2 cells ($\sim 1 \times 10^5$ per well) in 24-well plates
518 were transfected with 0.5, 1, or 2 μg of plasmid DNA per well using TransIT-LT1
519 transfection reagent in OptiMEM and incubated at 37°C for 3 h. Medium was removed
520 from the transfected cells and replaced with serum-free MEM for 1 h prior to virus
521 adsorption. SA11 rotavirus was activated by incubation with 1 $\mu\text{g}/\text{ml}$ trypsin at 37°C for
522 1 h. Medium was removed from the cells, and they were adsorbed with activated SA11
523 rotavirus diluted in 0.1 ml of serum-free MEM per well to a MOI of 0.1 PFU/cell at 37°C
524 for 1 h. After adsorption, cells were washed then incubated in serum-free MEM
525 containing 0.5 $\mu\text{g}/\text{ml}$ of trypsin at 37°C for 16 h. Cell lysates were harvested after three
526 rounds of freezing and thawing, and virus in the resultant lysates was quantified by FFA.

527 For longer-term rotavirus transfection-infection experiments, Caco-2 cells ($\sim 1 \times$
528 10^5 per well) in 24-well plates were transfected with 1 μg of plasmid DNA per well using
529 TransIT-LT1 transfection reagent in OptiMEM and incubated at 37°C for 3 h. Medium
530 was removed from the transfected cells and replaced with serum-free MEM for 1 h prior
531 to virus adsorption. SA11 rotavirus was activated by incubation with 1 $\mu\text{g}/\text{ml}$ trypsin at
532 37°C for 1 h. Medium was removed from the cells, and they were adsorbed with
533 activated SA11 rotavirus diluted in 0.1 ml of serum-free MEM per well to a MOI of 1

534 PFU/cell at 37°C for 1 h. After adsorption, cells were washed then incubated in MEM
535 containing 20% FBS at 37°C for 24 or 48 h. Cell lysates were harvested after three
536 rounds of freezing and thawing, and virus in the resultant lysates was quantified by FFA.

537 **Transfection-Infection Experiments in 293T cells.** For short-term rotavirus
538 transfection-infection experiments, 293T cells ($\sim 2.5 \times 10^5$ per well) in 24-well plates
539 were transfected with 50, 10, or 2 ng of plasmid DNA per well using LyoVec and
540 incubated at 37°C for 3 h. Medium was removed from the transfected cells and replaced
541 with serum-free DMEM for 1 h prior to virus adsorption. SA11 rotavirus was activated by
542 incubation with 1 $\mu\text{g/ml}$ trypsin at 37°C for 1 h. Medium was removed from the cells, and
543 they were adsorbed with activated SA11 rotavirus diluted in 0.1 ml of serum-free DMEM
544 per well to a MOI of 1 PFU/cell at 37°C for 1 h. After adsorption, cells were washed then
545 incubated in serum-free DMEM containing 0.5 $\mu\text{g/ml}$ trypsin at 37°C for 16 h. Cell
546 lysates were harvested after three rounds of freezing and thawing, and virus in the
547 resultant lysates was quantified by FFA.

548 For longer-term rotavirus transfection-infection experiments, 293T cells ($\sim 2.5 \times$
549 10^5 per well) in 24-well plates were transfected with 6 ng of plasmid DNA per well using
550 LyoVec and incubated at 37°C for 3 h. Medium was removed from the transfected cells
551 and replaced with serum-free DMEM for 1 h prior to virus adsorption. SA11 rotavirus
552 was activated by incubation with 1 $\mu\text{g/ml}$ trypsin at 37°C for 1 h. Medium was removed
553 from the cells, and they were adsorbed with activated SA11 rotavirus diluted in 0.1 ml of
554 serum-free DMEM per well to a MOI of 0.1 PFU/cell at 37°C for 1 h. After adsorption,
555 cells were washed then incubated in DMEM containing 10% FBS at 37°C for 24 or 48 h.

556 Cell lysates were harvested after three rounds of freezing and thawing, and virus in the
557 resultant lysates was quantified by FFA.

558 **Fluorescent focus assay.** MA104 cells (4×10^5 per well) were seeded in black-
559 wall 96-well plates and incubated overnight until near confluency. Infected cell lysates
560 were activated with 1 $\mu\text{g/ml}$ trypsin for at 37°C for 1 h then serially diluted in serum-free
561 MEM. Medium was removed from MA104 cells, they were washed twice in serum-free
562 MEM and adsorbed with serial virus dilutions at 37°C for 1 h. Inocula were removed,
563 cells were washed with serum-free MEM then incubated in fresh medium at 37°C for 14-
564 18 h. Cells were fixed with cold methanol, and rotavirus proteins were detected by
565 incubation with sheep polyclonal rotavirus antiserum at a 1:500 dilution in PBS
566 containing 0.5% Triton X-100 at 37°C, followed by incubation with Alexa Fluor 488-
567 conjugated anti-sheep IgG diluted 1:1000 and 300 nM DAPI. Images were captured for
568 four fields of view per well using an ImageXpress Micro XL automated microscope
569 imager (Molecular Devices). Total and percent infected cells were quantified using
570 MetaXpress high-content image acquisition and analysis software (Molecular Devices).
571 Fluorescent foci from four fields of view in duplicate wells for each sample were
572 quantified. Statistical analyses were performed using GraphPad Prism 7 (GraphPad).
573 Virus titers in cells transfected with plasmids expressing NBV p10 or RBV NSP1-1 were
574 compared to those in vector-transfected cells using an unpaired t-test.

575 **Amino acid alignments and phylogenetic analysis.** Sequences of NSP1-1
576 were obtained from GenBank. Accession numbers for FAST sequences analyzed for
577 the ML tree shown in [Fig. 3A](#) and alignment in [Fig. 3B](#) are ACN38055, ADZ31982,
578 ABV01045, AAM92750, AAM92738, AAF45151, ABY78878, AAF45157.1, ABM67655,

579 ACU68609, AAP03134, AHL26969, and AAL01373. Accession numbers for rotavirus
580 segment 5 source sequences for NSP1-1 proteins analyzed for the ML tree shown in
581 [Fig. 3A](#) are KY689691, NC_021546, KX362373, KC876005, NC_021583, NC_026820,
582 and KY026790. In each case, the smaller ORF sequence was analyzed. Accession
583 numbers for rotavirus segment 5 source sequences for NSP1-1 proteins in [Figs. 3B and](#)
584 [S1](#) are indicated.

585 For phylogenetic analysis, amino acid sequences were aligned using the
586 MUSCLE algorithm in MEGA 7.0 (62). The Le Gascuel 2008 model (63) was selected
587 as the best-fit model by Modeltest and used in maximum likelihood (ML) phylogeny
588 construction with 1000 bootstrap replicates (in MEGA 7.0). Initial tree(s) for the heuristic
589 search were obtained automatically by applying Neighbor-Join and BioNJ algorithms to
590 a matrix of pairwise distances estimated using a JTT model, and then selecting the
591 topology with superior log likelihood value. A discrete Gamma distribution was used to
592 model evolutionary rate differences among sites (5 categories (+G, parameter =
593 8.9228)). The tree with the highest log likelihood is shown in [Fig. 3A](#). The ML tree was
594 visualized using FigTree v1.4.2 (<http://tree.bio.ed.ac.uk/software/figtree/>).

595 For [Figs. 3B and S1](#), amino acid alignments were constructed with MAFFT v7.2
596 (64) using the E-INS-I strategy. N-myristylation motifs were defined using ScanProsite
597 (65). Transmembrane helices were predicted with the TMHMM Server v2.0
598 (www.cbs.dtu.dk/services/TMHMM/). Hydrophobic, polybasic, and polyproline regions
599 for FAST proteins were identified previously (31). Hydrophobic patches for NSP1-1
600 proteins were identified using ProtScale, with a window size of nine amino acids (66).
601 Polybasic regions for NSP1-1 proteins were identified visually.

602

603 **ACKNOWLEDGEMENTS**

604 We thank Dr. Takeshi Kobayashi for NBV p10 in pCAGGS and Dr. Marco Morelli
605 for pLIC6 and pLIC8 plasmids.

606 This research was supported in part by CTSA award No. UL1 TR002243 from
607 the National Center for Advancing Translational Sciences. Its contents are solely the
608 responsibility of the authors and do not necessarily represent official views of the
609 National Center for Advancing Translational Sciences or the National Institutes of
610 Health.

611 REFERENCES

- 612 1. **Estes MK, Greenberg HB.** 2013. Rotaviruses, p 1347-1401. *In* Knipe DM,
613 Howley PM (ed), Fields Virology, Sixth ed, vol 2. Lippincott Williams & Wilkins,
614 Philadelphia.
- 615 2. **Ding S, Zhu S, Ren L, Feng N, Song Y, Ge X, Li B, Flavell RA, Greenberg**
616 **HB.** 2018. Rotavirus VP3 targets MAVS for degradation to inhibit type III
617 interferon expression in intestinal epithelial cells. *Elife* **7**.
- 618 3. **Morelli M, Ogden KM, Patton JT.** 2015. Silencing the alarms: Innate immune
619 antagonism by rotavirus NSP1 and VP3. *Virology* **479-480**:75-84.
- 620 4. **International Committee on Taxonomy of Viruses., King AMQ.** 2012. Virus
621 taxonomy : classification and nomenclature of viruses : ninth report of the
622 International Committee on Taxonomy of Viruses. Academic Press, London ;
623 Waltham, MA.
- 624 5. **Ogden KM, Johne R, Patton JT.** 2012. Rotavirus RNA polymerases resolve into
625 two phylogenetically distinct classes that differ in their mechanism of template
626 recognition. *Virology* **431**:50-57.
- 627 6. **Matthijssens J, Otto PH, Ciarlet M, Desselberger U, Van Ranst M, Johne R.**
628 2012. VP6-sequence-based cutoff values as a criterion for rotavirus species
629 demarcation. *Arch Virol* **157**:1177-1182.
- 630 7. **Dhama K, Chauhan RS, Mahendran M, Malik SV.** 2009. Rotavirus diarrhea in
631 bovines and other domestic animals. *Vet Res Commun* **33**:1-23.
- 632 8. **Martella V, Banyai K, Matthijssens J, Buonavoglia C, Ciarlet M.** 2010.
633 Zoonotic aspects of rotaviruses. *Vet Microbiol* **140**:246-255.

- 634 9. **Doro R, Farkas SL, Martella V, Banyai K.** 2015. Zoonotic transmission of
635 rotavirus: surveillance and control. *Expert Rev Anti Infect Ther* **13**:1337-1350.
- 636 10. **Brown DW, Beards GM, Chen GM, Flewett TH.** 1987. Prevalence of antibody
637 to group B (atypical) rotavirus in humans and animals. *J Clin Microbiol* **25**:316-
638 319.
- 639 11. **Marthaler D, Rossow K, Culhane M, Goyal S, Collins J, Matthijssens J,**
640 **Nelson M, Ciarlet M.** 2014. Widespread rotavirus H in commercially raised pigs,
641 United States. *Emerg Infect Dis* **20**:1195-1198.
- 642 12. **Marthaler D, Rossow K, Gramer M, Collins J, Goyal S, Tsunemitsu H, Kuga**
643 **K, Suzuki T, Ciarlet M, Matthijssens J.** 2012. Detection of substantial porcine
644 group B rotavirus genetic diversity in the United States, resulting in a modified
645 classification proposal for G genotypes. *Virology* **433**:85-96.
- 646 13. **Joshi MS, Ganorkar NN, Ranshing SS, Basu A, Chavan NA, Gopalkrishna V.**
647 2017. Identification of group B rotavirus as an etiological agent in the
648 gastroenteritis outbreak in Maharashtra, India. *J Med Virol* **89**:2244-2248.
- 649 14. **Krishnan T, Sen A, Choudhury JS, Das S, Naik TN, Bhattacharya SK.** 1999.
650 Emergence of adult diarrhoea rotavirus in Calcutta, India. *Lancet* **353**:380-381.
- 651 15. **Lahon A, Maniya NH, Tambe GU, Chinchole PR, Purwar S, Jacob G,**
652 **Chitambar SD.** 2013. Group B rotavirus infection in patients with acute
653 gastroenteritis from India: 1994-1995 and 2004-2010. *Epidemiol Infect* **141**:969-
654 975.

- 655 16. **Sanekata T, Ahmed MU, Kader A, Taniguchi K, Kobayashi N.** 2003. Human
656 group B rotavirus infections cause severe diarrhea in children and adults in
657 Bangladesh. *J Clin Microbiol* **41**:2187-2190.
- 658 17. **Chen CM, Hung T, Bridger JC, McCrae MA.** 1985. Chinese adult rotavirus is a
659 group B rotavirus. *Lancet* **2**:1123-1124.
- 660 18. **Eiden J, Vonderfecht S, Yolken RH.** 1985. Evidence that a novel rotavirus-like
661 agent of rats can cause gastroenteritis in man. *Lancet* **2**:8-11.
- 662 19. **Hung T, Chen GM, Wang CG, Chou ZY, Chao TX, Ye WW, Yao HL, Meng KH.**
663 1983. Rotavirus-like agent in adult non-bacterial diarrhoea in China. *Lancet*
664 **2**:1078-1079.
- 665 20. **Hung T, Chen GM, Wang CG, Yao HL, Fang ZY, Chao TX, Chou ZY, Ye W,**
666 **Chang XJ, Den SS, et al.** 1984. Waterborne outbreak of rotavirus diarrhoea in
667 adults in China caused by a novel rotavirus. *Lancet* **1**:1139-1142.
- 668 21. **Sen A, Kobayashi N, Das S, Krishnan T, Bhattacharya SK, Naik TN.** 2001.
669 The evolution of human group B rotaviruses. *Lancet* **357**:198-199.
- 670 22. **Saiada F, Rahman HN, Moni S, Karim MM, Pourkarim MR, Azim T, Rahman**
671 **M.** 2011. Clinical presentation and molecular characterization of group B
672 rotaviruses in diarrhoea patients in Bangladesh. *J Med Microbiol* **60**:529-536.
- 673 23. **Alam MM, Pun SB, Gauchan P, Yokoo M, Doan YH, Tran TN, Nakagomi T,**
674 **Nakagomi O, Pandey BD.** 2013. The first identification of rotavirus B from
675 children and adults with acute diarrhoea in kathmandu, Nepal. *Trop Med Health*
676 **41**:129-134.

- 677 24. **Eiden JJ, Mouzinho A, Lindsay DA, Glass RI, Fang ZY, Taylor JL.** 1994.
678 Serum antibody response to recombinant major inner capsid protein following
679 human infection with group B rotavirus. *J Clin Microbiol* **32**:1599-1603.
- 680 25. **Nakata S, Estes MK, Graham DY, Wang SS, Gary GW, Melnick JL.** 1987.
681 Detection of antibody to group B adult diarrhea rotaviruses in humans. *J Clin*
682 *Microbiol* **25**:812-818.
- 683 26. **Suzuki T, Kuga K, Miyazaki A, Tsunemitsu H.** 2011. Genetic divergence and
684 classification of non-structural protein 1 among porcine rotaviruses of species B.
685 *J Gen Virol* **92**:2922-2929.
- 686 27. **Fang ZY, Glass RI, Penaranda M, Dong H, Monroe SS, Wen L, Estes MK,**
687 **Eiden J, Yolken RH, Saif L, et al.** 1989. Purification and characterization of
688 adult diarrhea rotavirus: identification of viral structural proteins. *J Virol* **63**:2191-
689 2197.
- 690 28. **Fang ZY, Monroe SS, Dong H, Penaranda M, Wen L, Gouvea V, Allen JR,**
691 **Hung T, Glass RI.** 1992. Coding assignments of the genome of adult diarrhea
692 rotavirus. *Arch Virol* **125**:53-69.
- 693 29. **Eiden JJ.** 1994. Expression and sequence analysis of gene 7 of the IDIR agent
694 (group B rotavirus): similarity with NS53 of group A rotavirus. *Virology* **199**:212-
695 218.
- 696 30. **Boutillier J, Duncan R.** 2011. The reovirus fusion-associated small
697 transmembrane (FAST) proteins: virus-encoded cellular fusogens. *Curr Top*
698 *Membr* **68**:107-140.

- 699 31. **Ciechonska M, Duncan R.** 2014. Reovirus FAST proteins: virus-encoded
700 cellular fusogens. *Trends Microbiol* **22**:715-724.
- 701 32. **Kanai Y, Komoto S, Kawagishi T, Nouda R, Nagasawa N, Onishi M,**
702 **Matsuura Y, Taniguchi K, Kobayashi T.** 2017. Entirely plasmid-based reverse
703 genetics system for rotaviruses. *Proc Natl Acad Sci U S A* **114**:2349-2354.
- 704 33. **Kanai Y, Kawagishi T, Sakai Y, Nouda R, Shimojima M, Saijo M, Matsuura Y,**
705 **Kobayashi T.** 2019. Cell-cell fusion induced by reovirus FAST proteins
706 enhances replication and pathogenicity of non-enveloped dsRNA viruses. *PLoS*
707 *Pathog* **15**:e1007675.
- 708 34. **Key T, Duncan R.** 2014. A compact, multifunctional fusion module directs
709 cholesterol-dependent homomultimerization and syncytiogenic efficiency of
710 reovirus p10 FAST proteins. *PLoS Pathog* **10**:e1004023.
- 711 35. **Salsman J, Top D, Boutilier J, Duncan R.** 2005. Extensive syncytium formation
712 mediated by the reovirus FAST proteins triggers apoptosis-induced membrane
713 instability. *J Virol* **79**:8090-8100.
- 714 36. **Corcoran JA, Duncan R.** 2004. Reptilian reovirus utilizes a small type III protein
715 with an external myristylated amino terminus to mediate cell-cell fusion. *J Virol*
716 **78**:4342-4351.
- 717 37. **Corcoran JA, Syvitski R, Top D, Epand RM, Epand RF, Jakeman D, Duncan**
718 **R.** 2004. Myristoylation, a protruding loop, and structural plasticity are essential
719 features of a nonenveloped virus fusion peptide motif. *J Biol Chem* **279**:51386-
720 51394.

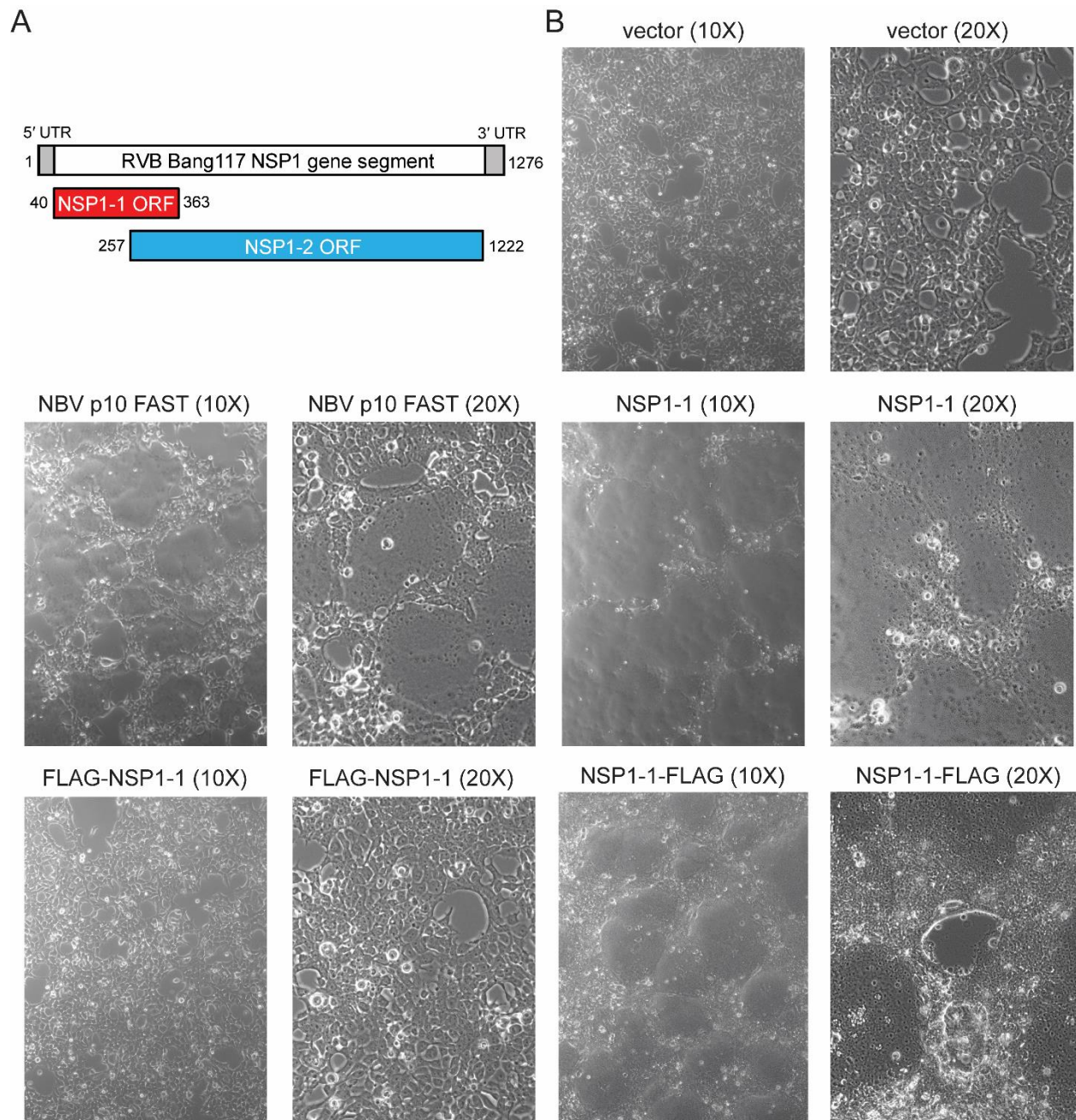
- 721 38. **Dawe S, Corcoran JA, Clancy EK, Salsman J, Duncan R.** 2005. Unusual
722 topological arrangement of structural motifs in the baboon reovirus fusion-
723 associated small transmembrane protein. *J Virol* **79**:6216-6226.
- 724 39. **Dawe S, Duncan R.** 2002. The S4 genome segment of baboon reovirus is
725 bicistronic and encodes a novel fusion-associated small transmembrane protein.
726 *J Virol* **76**:2131-2140.
- 727 40. **Shmulevitz M, Epand RF, Epand RM, Duncan R.** 2004. Structural and
728 functional properties of an unusual internal fusion peptide in a nonenveloped
729 virus membrane fusion protein. *J Virol* **78**:2808-2818.
- 730 41. **Barry C, Key T, Haddad R, Duncan R.** 2010. Features of a spatially constrained
731 cystine loop in the p10 FAST protein ectodomain define a new class of viral
732 fusion peptides. *J Biol Chem* **285**:16424-16433.
- 733 42. **Key T, Sarker M, de Antueno R, Rainey JK, Duncan R.** 2015. The p10 FAST
734 protein fusion peptide functions as a cystine noose to induce cholesterol-
735 dependent liposome fusion without liposome tubulation. *Biochim Biophys Acta*
736 **1848**:408-416.
- 737 43. **Shmulevitz M, Salsman J, Duncan R.** 2003. Palmitoylation, membrane-
738 proximal basic residues, and transmembrane glycine residues in the reovirus p10
739 protein are essential for syncytium formation. *J Virol* **77**:9769-9779.
- 740 44. **Shmulevitz M, Duncan R.** 2000. A new class of fusion-associated small
741 transmembrane (FAST) proteins encoded by the non-enveloped fusogenic
742 reoviruses. *EMBO J* **19**:902-912.

- 743 45. **Parmar HB, Barry C, Duncan R.** 2014. Polybasic trafficking signal mediates
744 golgi export, ER retention or ER export and retrieval based on membrane-
745 proximity. PLoS One **9**:e94194.
- 746 46. **Parmar HB, Duncan R.** 2016. A novel tribasic Golgi export signal directs cargo
747 protein interaction with activated Rab11 and AP-1-dependent Golgi-plasma
748 membrane trafficking. Mol Biol Cell **27**:1320-1331.
- 749 47. **Parmar HB, Barry C, Kai F, Duncan R.** 2014. Golgi complex-plasma membrane
750 trafficking directed by an autonomous, tribasic Golgi export signal. Mol Biol Cell
751 **25**:866-878.
- 752 48. **Clancy EK, Duncan R.** 2009. Reovirus FAST protein transmembrane domains
753 function in a modular, primary sequence-independent manner to mediate cell-cell
754 membrane fusion. J Virol **83**:2941-2950.
- 755 49. **Salim AF, Phillips AD, Walker-Smith JA, Farthing MJ.** 1995. Sequential
756 changes in small intestinal structure and function during rotavirus infection in
757 neonatal rats. Gut **36**:231-238.
- 758 50. **Vonderfecht SL, Huber AC, Eiden J, Mader LC, Yolken RH.** 1984. Infectious
759 diarrhea of infant rats produced by a rotavirus-like agent. J Virol **52**:94-98.
- 760 51. **Theil KW, Grooms DL, McCloskey CM, Redman DR.** 1995. Group B rotavirus
761 associated with an outbreak of neonatal lamb diarrhea. J Vet Diagn Invest **7**:148-
762 150.
- 763 52. **Sanekata T, Kuwamoto Y, Akamatsu S, Sakon N, Oseto M, Taniguchi K,**
764 **Nakata S, Estes MK.** 1996. Isolation of group B porcine rotavirus in cell culture.
765 J Clin Microbiol **34**:759-761.

- 766 53. **Salsman J, Top D, Barry C, Duncan R.** 2008. A virus-encoded cell-cell fusion
767 machine dependent on surrogate adhesins. *PLoS Pathog* **4**:e1000016.
- 768 54. **Hayashi M, Murakami T, Kuroda Y, Takai H, Ide H, Awang A, Suzuki T,**
769 **Miyazaki A, Nagai M, Tsunemitsu H.** 2016. Reinfection of adult cattle with
770 rotavirus B during repeated outbreaks of epidemic diarrhea. *Can J Vet Res*
771 **80**:189-196.
- 772 55. **Velazquez FR, Matson DO, Calva JJ, Guerrero L, Morrow AL, Carter-**
773 **Campbell S, Glass RI, Estes MK, Pickering LK, Ruiz-Palacios GM.** 1996.
774 Rotavirus infection in infants as protection against subsequent infections. *N Engl*
775 *J Med* **335**:1022-1028.
- 776 56. **Arnold MM.** 2016. The Rotavirus Interferon Antagonist NSP1: Many Targets,
777 Many Questions. *J Virol* **90**:5212-5215.
- 778 57. **Nibert ML, Duncan R.** 2013. Bioinformatics of recent aqua- and orthoreovirus
779 isolates from fish: evolutionary gain or loss of FAST and fiber proteins and
780 taxonomic implications. *PLoS One* **8**:e68607.
- 781 58. **Saxena K, Blutt SE, Ettayebi K, Zeng XL, Broughman JR, Crawford SE,**
782 **Karandikar UC, Sastri NP, Conner ME, Opekun AR, Graham DY, Qureshi W,**
783 **Sherman V, Foulke-Abel J, In J, Kovbasnjuk O, Zachos NC, Donowitz M,**
784 **Estes MK.** 2016. Human Intestinal Enteroids: a New Model To Study Human
785 Rotavirus Infection, Host Restriction, and Pathophysiology. *J Virol* **90**:43-56.
- 786 59. **Kobayashi T, Ooms LS, Ikizler M, Chappell JD, Dermody TS.** 2010. An
787 improved reverse genetics system for mammalian orthoreoviruses. *Virology*
788 **398**:194-200.

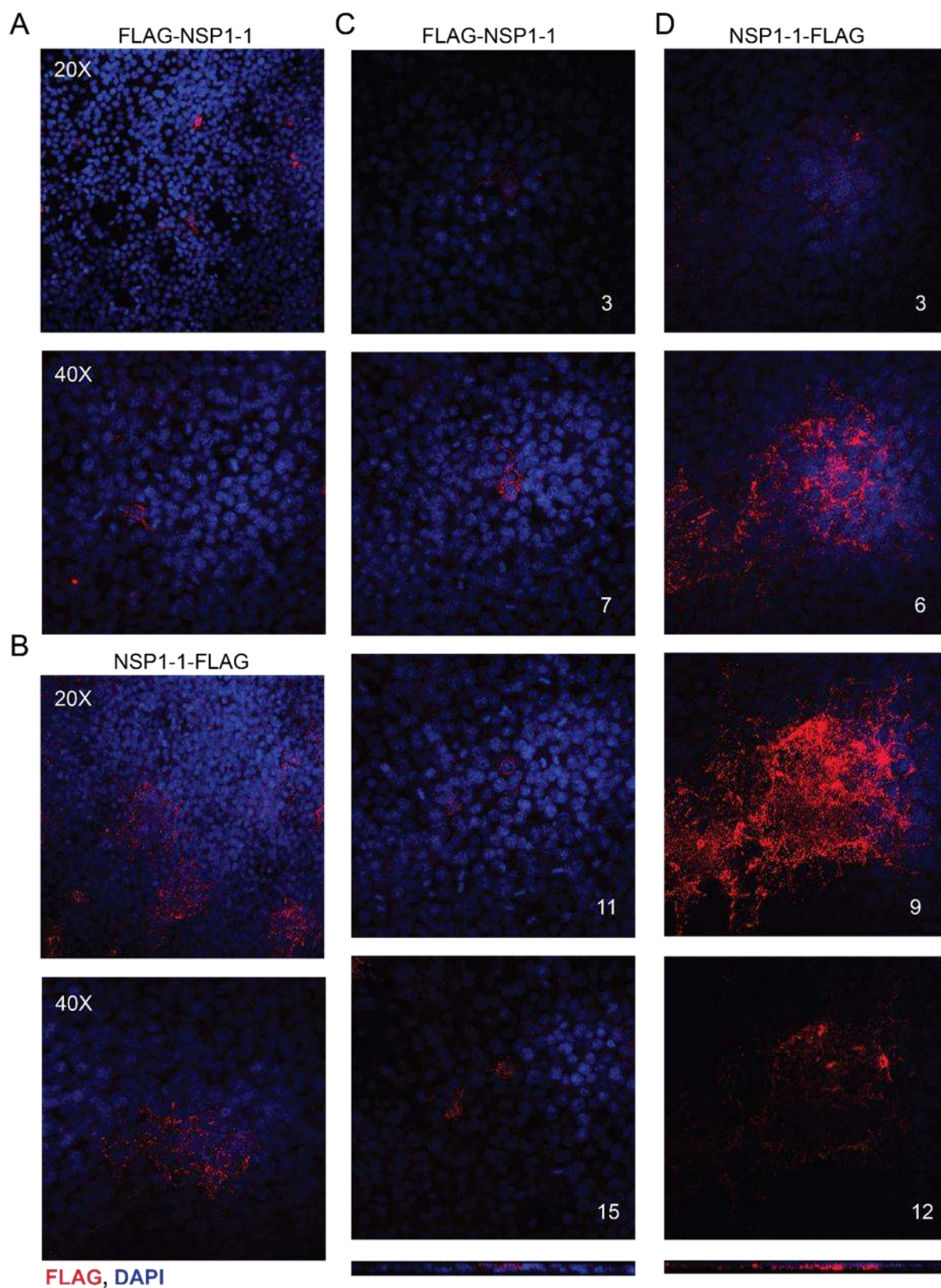
- 789 60. **Arnold M, Patton JT, McDonald SM.** 2009. Culturing, storage, and
790 quantification of rotaviruses. *Curr Protoc Microbiol* **Chapter 15**:Unit 15C 13.
- 791 61. **Yamamoto D, Ghosh S, Ganesh B, Krishnan T, Chawla-Sarkar M, Alam MM,**
792 **Aung TS, Kobayashi N.** 2010. Analysis of genetic diversity and molecular
793 evolution of human group B rotaviruses based on whole genome segments. *J*
794 *Gen Virol* **91**:1772-1781.
- 795 62. **Kumar S, Stecher G, Tamura K.** 2016. MEGA7: Molecular Evolutionary
796 Genetics Analysis Version 7.0 for Bigger Datasets. *Mol Biol Evol* **33**:1870-1874.
- 797 63. **Le SQ, Gascuel O.** 2008. An improved general amino acid replacement matrix.
798 *Mol Biol Evol* **25**:1307-1320.
- 799 64. **Katoh K, Standley DM.** 2013. MAFFT multiple sequence alignment software
800 version 7: improvements in performance and usability. *Mol Biol Evol* **30**:772-780.
- 801 65. **de Castro E, Sigrist CJ, Gattiker A, Bulliard V, Langendijk-Genevaux PS,**
802 **Gasteiger E, Bairoch A, Hulo N.** 2006. ScanProsite: detection of PROSITE
803 signature matches and ProRule-associated functional and structural residues in
804 proteins. *Nucleic Acids Res* **34**:W362-365.
- 805 66. **Gasteiger E, Hoogland C, Gattiker A, Duvaud S, Wilkins MR, Appel RD,**
806 **Bairoch A.** 2005. Protein Identification and Analysis Tools on the ExPASy
807 Server, p 571 - 607. *In* Walker JM (ed), *The Proteomics Protocols Handbook*.
808 Humana Press.
- 809
- 810

811 FIGURE LEGENDS



812

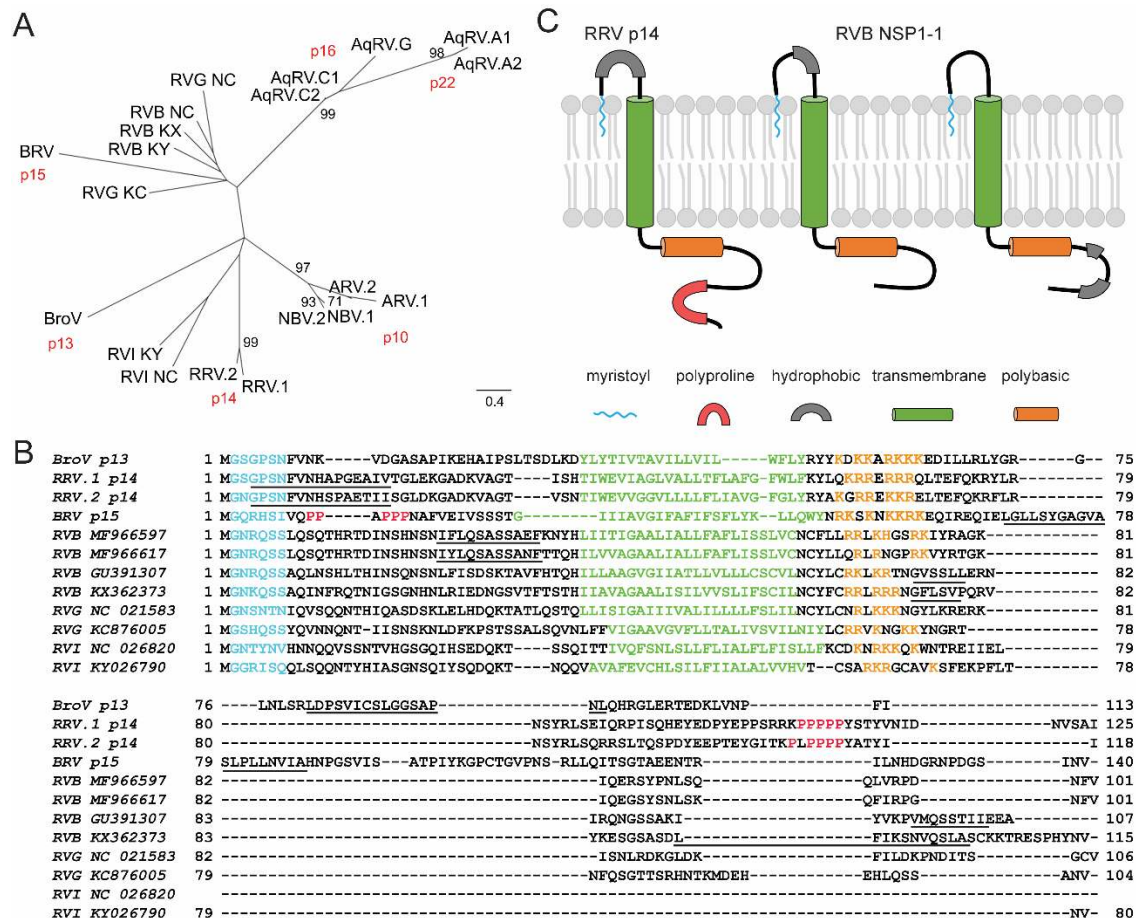
813 **Figure 1.** RVB Bang117 NSP1-1 mediates syncytia formation in 293T cells. (A)
814 Schematic showing the organization of RVB Bang117 NSP1 gene segment, including
815 untranslated regions (UTRs) and two putative ORFs. (B) Differential interference
816 contrast images of 293T cells transfected with vector alone or plasmids encoding NBV
817 p10 FAST or RVB Bang117 NSP1-1 in its untagged form or with an N- or C-terminal
818 FLAG tag. Representative images are shown. Plasmids used for transfection and
819 objective lens magnification are indicated.



820

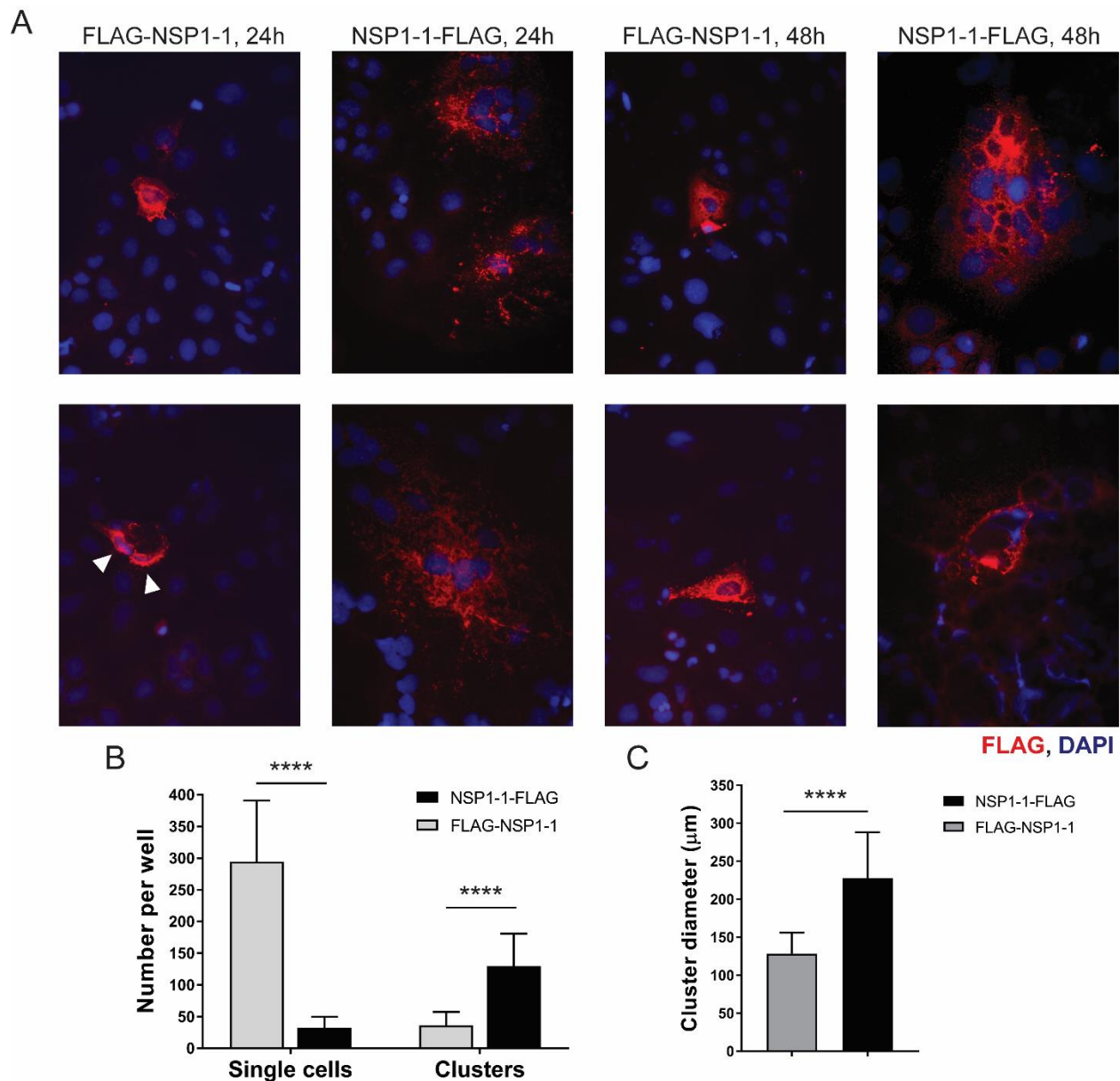
821 **Figure 2.** RVB Bang117 NSP1-1 localization in 293T cells. 293T cells were transfected
822 with plasmids encoding RVB Bang117 NSP1-1 with an N- or C-terminal FLAG tag, as

823 indicated. Cells were fixed and stained with antibodies to detect FLAG (red) or nuclei
824 (blue) and imaged using confocal microscopy. (A-B) Images from a single confocal
825 plane of 293T cells transfected with plasmids encoding FLAG-NSP1-1 (A) or NSP1-1-
826 FLAG (B) taken using the 20X or 40X objective, as indicated. (C-D) Confocal images
827 from comparable focal planes in a Z-stack taken using the 40X objective for 293T cells
828 transfected with plasmids encoding FLAG-NSP1-1 (B) or NSP1-1-FLAG (C). Z-section
829 number is indicated; numbers increase coincident with distance from the adherent
830 surface of the monolayer. Bars at the bottom represent orthogonal views through the Z-
831 stack, approximately at the center of the images.
832



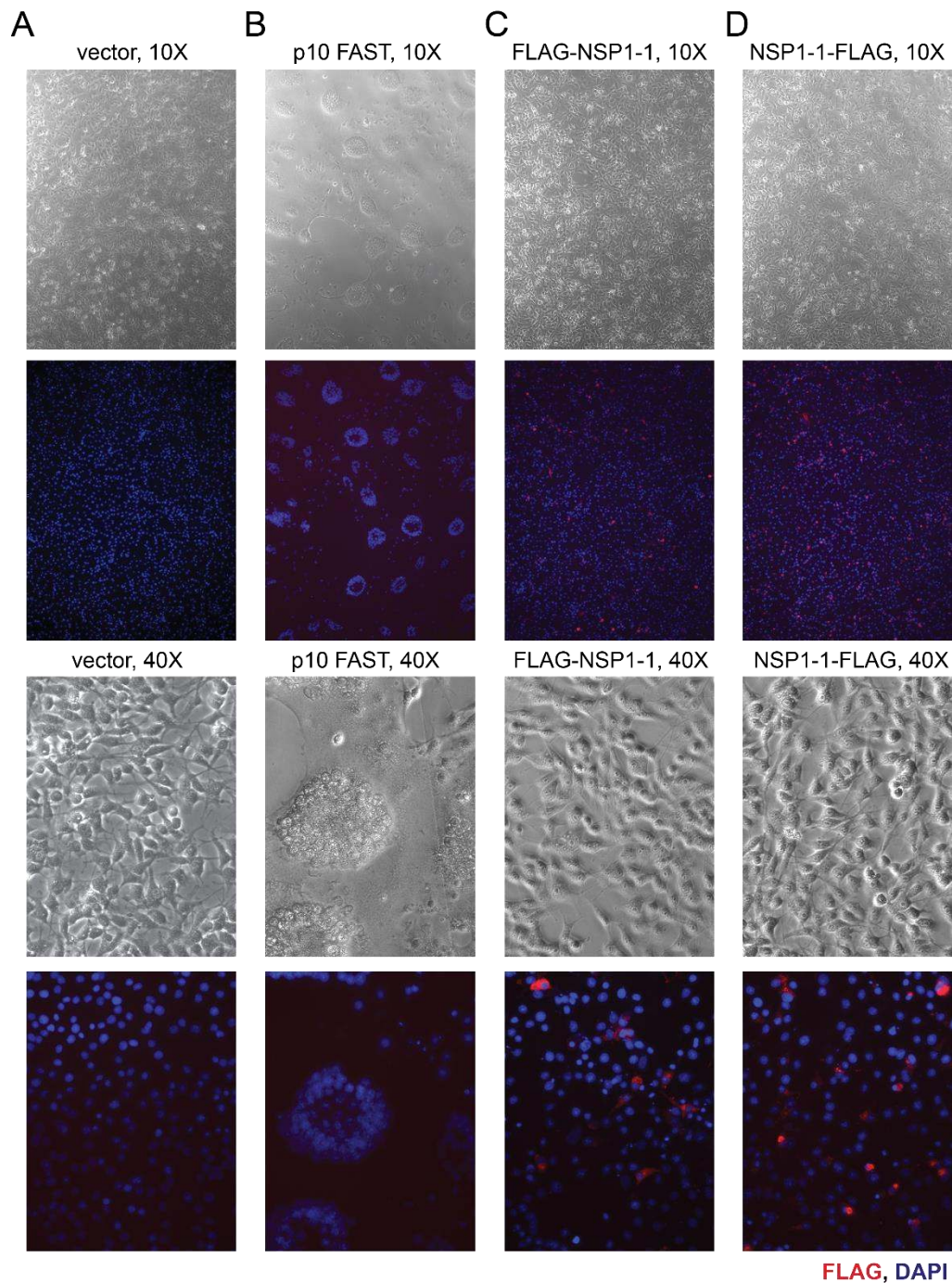
833

834 **Figure 3.** Conserved features of *Reoviridae* FAST proteins. (A) Maximum likelihood tree
835 showing relationships among *Reoviridae* FAST and rotavirus NSP1-1 proteins.
836 Abbreviations are: AqRV.A1, Atlantic salmon aquareovirus; AqRV.A2, Turbot
837 aquareovirus; AqRV.G, American grass carp aquareovirus; AqRV.C1, Golden shiner
838 aquareovirus; AqRV.C2, Grass carp aquareovirus; ARV.1, Avian orthoreovirus 176;
839 ARV.2, Psittacine orthoreovirus; NBV.1, Nelson Bay orthoreovirus; NBV.2, Melaka
840 orthoreovirus; BroV, Broome orthoreovirus; RRV.1, Python orthoreovirus; RRV.2, Green
841 bush viper orthoreovirus; BRV, Baboon orthoreovirus; RVB KY, Rotavirus B strain
842 RVB/Goat-wt/USA/Minnesota-1/2016; RVB KX, Rotavirus B strain RVB/Pig-
843 wt/VNM/12089_7; RVB NC, Human rotavirus B strain Bang373; RVG KC, Rotavirus G
844 pigeon/HK18; RVG NC, Rotavirus G chicken/03V0567/DEU/2003; RVI NC, Rotavirus I
845 strain KE135/2012; RVI KY, Rotavirus I cat. Scale, in amino acid substitutions per site,
846 is indicated. (B) Alignment of selected *Reoviridae* FAST and rotavirus NSP1-1 proteins.
847 Abbreviations for FAST proteins are as in (A). Rotavirus species (RVB, RVG, or RVI)
848 and accession number are indicated. Predicted N-myristoylation motifs are colored
849 cyan, transmembrane helices are colored green, polybasic regions are colored orange,
850 polyproline regions are colored red, and hydrophobic regions are underlined. (C)
851 Cartoon models highlighting the predicted features and membrane topology for the RRV
852 p14 FAST protein and for RVB NSP1-1. Features and models of BroV p13, RRV p14,
853 and BRV p15 shown in (B) and (C) are based on previously published work (31).



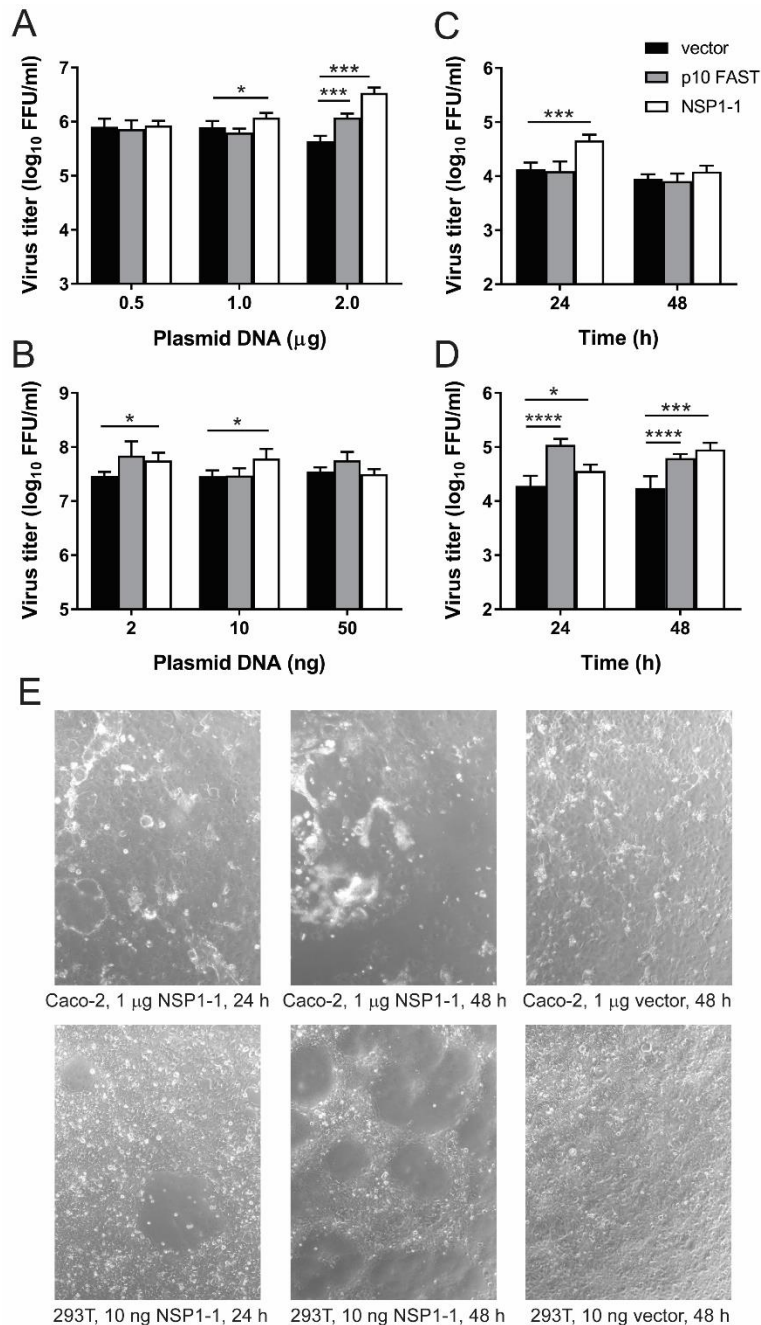
854

855 **Figure 4.** RVB Bang117 FAST mediates syncytia formation in Caco-2 cells. Caco-2
856 cells in 24-well plates were transfected with plasmids encoding RVB Bang117 NSP1-1
857 with an N- or C-terminal FLAG tag. Cells were fixed and stained with antibodies to
858 detect FLAG (red) or nuclei (blue) and imaged using immunofluorescence microscopy
859 at 24 and 48 h post transfection. (A) Representative images are shown. White triangles
860 indicate adjacent FLAG-positive FLAG-NSP1-1-transfected cells. (B) The numbers of
861 FLAG-positive clusters (3 or more adjacent cells) and FLAG-positive single cells per
862 well were quantified in three wells per experiment in four independent experiments. $n =$
863 12. (C) The diameters of 20 FLAG-positive clusters per experiment in four independent
864 experiments were quantified. $n = 80$. ****, $p < 0.0001$ by unpaired t test.



865

866 **Figure 5.** RVB NSP1-1 fails to mediate fusion and exhibits perinuclear localization in
867 BHK cells. BHK-T7 cells were transfected with vector alone (A) or plasmids encoding
868 NBV p10 FAST (B) or RVB Bang117 NSP1-1 with an N-terminal (C) or C-terminal (D)
869 FLAG tag. Cells were fixed and stained with antibodies to detect FLAG (red) or nuclei
870 (blue) and imaged using both differential interference contrast and immunofluorescence
871 microscopy. Representative images are shown. Plasmids used for transfection and
872 objective lens magnification are indicated.



873

874 **Figure 6.** RVB Bang117 FAST mediates enhanced rotavirus replication in human cells.
 875 (A-B) Short-term infection. Caco-2 cells (A) or 293T cells (B) were transfected with the
 876 indicated amount of plasmid DNA. At 4 h post transfection, cells were adsorbed with
 877 trypsin-activated SA11 rotavirus, washed, incubated in serum-free medium containing
 878 trypsin at 37°C for 16 h, and lysed. Virus titers in cell lysates were quantified by FFA.
 879 (C-D) Rotavirus spread in the presence of FBS. Caco-2 cells were transfected with 1 μg
 880 of plasmid DNA (C), or 293T cells were transfected with 10 ng of plasmid DNA (D). At 4
 881 h post transfection, cells were adsorbed with trypsin-activated SA11 rotavirus, washed,
 882 incubated in MEM containing 20% (Caco-2) or 10% (293T) FBS for 0, 24, or 48 h, and
 883 lysed. Virus titers in cell lysates were quantified by FFA. $n = 3$. *, $p < 0.05$; ***, $p < 0.001$;

884 ****, $p < 0.0001$ in comparison to vector alone by unpaired t test. (E) Cytopathic effects
885 in transfected cells. Caco-2 or 293T cells were transfected with the indicated
886 concentrations of plasmids and imaged using brightfield microscopy at 24 or 48 h post
887 transfection to reveal gross morphological changes in the monolayer.
888

889

```
Po RVB KY869733 1 MGNRQSSLSQSTHRDINDSHNSNIYLSQASSNEETQCHILVVAAGALIALFA--FLVSSLVNCFYLLRRLR--NGPRKIYRTCKIQEGSYSSLKQPIREDHFV----- 101
Po RVB MF966617 1 MGNRQSSLSQSTHRDINDSHNSNIYLSQASSNEETQCHILVVAAGALIALFA--FLVSSLVNCFYLLRRLR--NGPRKIYRTCKIQEGSYSSLKQPIREDHFV----- 101
Po RVB MF966616 1 MGNRQSSLSQSTHRDINDSHNSNIYLSQASSNEETQCHILVVAAGALIALFA--FLVSSLVNCFYLLRRLR--NGPRKIYRTCKIQEGSYSSLKQPIREDHFV----- 101
Po RVB KX362395 1 MGNRQSSLSQSTHRDINDSHNSNIYLSQASSNEETQCHILVVAAGALIALFA--FLVSSLVNCFYLLRRLR--NGPRKIYRTCKIQEGSYSSLKQPIREDHFV----- 101
Po RVB MF966615 1 MGNRQSSLSQSTHRDINDSHNSNIYLSQASSNEETQCHILVVAAGALIALFA--FLVSSLVNCFYLLRRLR--NGPRKIYRTCKIQEGSYSSLKQPIREDHFV----- 101
Po RVB MF966614 1 MGNRQSSLSQSTHRDINDSHNSNIYLSQASSNEETQCHILVVAAGALIALFA--FLVSSLVNCFYLLRRLR--NGPRKIYRTCKIQEGSYSSLKQPIREDHFV----- 101
Po RVB MF966613 1 MGNRQSSLSQSTHRDINDSHNSNIYLSQASSNEETQCHILVVAAGALIALFA--FLVSSLVNCFYLLRRLR--NGPRKIYRTCKIQEGSYSSLKQPIREDHFV----- 101
Po RVB MF966612 1 MGNRQSSLSQSTHRDINDSHNSNIYLSQASSNEETQCHILVVAAGALIALFA--FLVSSLVNCFYLLRRLR--NGPRKIYRTCKIQEGSYSSLKQPIREDHFV----- 101
Po RVB MF966611 1 MGNRQSSLSQSTHRDINDSHNSNIYLSQASSNEETQCHILVVAAGALIALFA--FLVSSLVNCFYLLRRLR--NGPRKIYRTCKIQEGSYSSLKQPIREDHFV----- 101
Po RVB MF966610 1 MGNRQSSLSQSTHRDINDSHNSNIYLSQASSNEETQCHILVVAAGALIALFA--FLVSSLVNCFYLLRRLR--NGPRKIYRTCKIQEGSYSSLKQPIREDHFV----- 101
Po RVB MF966609 1 MGNRQSSLSQSTHRDINDSHNSNIYLSQASSNEETQCHILVVAAGALIALFA--FLVSSLVNCFYLLRRLR--NGPRKIYRTCKIQEGSYSSLKQPIREDHFV----- 101
Po RVB MF966608 1 MGNRQSSLSQSTHRDINDSHNSNIYLSQASSNEETQCHILVVAAGALIALFA--FLVSSLVNCFYLLRRLR--NGPRKIYRTCKIQEGSYSSLKQPIREDHFV----- 101
Po RVB MF966607 1 MGNRQSSLSQSTHRDINDSHNSNIYLSQASSNEETQCHILVVAAGALIALFA--FLVSSLVNCFYLLRRLR--NGPRKIYRTCKIQEGSYSSLKQPIREDHFV----- 101
Po RVB MF966606 1 MGNRQSSLSQSTHRDINDSHNSNIYLSQASSNEETQCHILVVAAGALIALFA--FLVSSLVNCFYLLRRLR--NGPRKIYRTCKIQEGSYSSLKQPIREDHFV----- 101
Po RVB MF966605 1 MGNRQSSLSQSTHRDINDSHNSNIYLSQASSNEETQCHILVVAAGALIALFA--FLVSSLVNCFYLLRRLR--NGPRKIYRTCKIQEGSYSSLKQPIREDHFV----- 101
Po RVB MF966604 1 MGNRQSSLSQSTHRDINDSHNSNIYLSQASSNEETQCHILVVAAGALIALFA--FLVSSLVNCFYLLRRLR--NGPRKIYRTCKIQEGSYSSLKQPIREDHFV----- 101
Po RVB MF966603 1 MGNRQSSLSQSTHRDINDSHNSNIYLSQASSNEETQCHILVVAAGALIALFA--FLVSSLVNCFYLLRRLR--NGPRKIYRTCKIQEGSYSSLKQPIREDHFV----- 101
Po RVB MF966602 1 MGNRQSSLSQSTHRDINDSHNSNIYLSQASSNEETQCHILVVAAGALIALFA--FLVSSLVNCFYLLRRLR--NGPRKIYRTCKIQEGSYSSLKQPIREDHFV----- 101
Po RVB MF966601 1 MGNRQSSLSQSTHRDINDSHNSNIYLSQASSNEETQCHILVVAAGALIALFA--FLVSSLVNCFYLLRRLR--NGPRKIYRTCKIQEGSYSSLKQPIREDHFV----- 101
Po RVB MF966600 1 MGNRQSSLSQSTHRDINDSHNSNIYLSQASSNEETQCHILVVAAGALIALFA--FLVSSLVNCFYLLRRLR--NGPRKIYRTCKIQEGSYSSLKQPIREDHFV----- 101
Po RVB MF966599 1 MGNRQSSLSQSTHRDINDSHNSNIYLSQASSNEETQCHILVVAAGALIALFA--FLVSSLVNCFYLLRRLR--NGPRKIYRTCKIQEGSYSSLKQPIREDHFV----- 101
Po RVB MF966598 1 MGNRQSSLSQSTHRDINDSHNSNIYLSQASSNEETQCHILVVAAGALIALFA--FLVSSLVNCFYLLRRLR--NGPRKIYRTCKIQEGSYSSLKQPIREDHFV----- 101
Po RVB MF966597 1 MGNRQSSLSQSTHRDINDSHNSNIYLSQASSNEETQCHILVVAAGALIALFA--FLVSSLVNCFYLLRRLR--NGPRKIYRTCKIQEGSYSSLKQPIREDHFV----- 101
Cp RVB KY686596 1 MGSSDSSLSQSVHSHNHSQSSIHLOGTSTANTTCHILVVAAGALIALFA--FLVSSLVNCFYLLRRLR--NGPRKIYRTCKIQEGSYSSLKQPIREDHFV----- 101
Cp RVB KY686595 1 MGSSDSSLSQSVHSHNHSQSSIHLOGTSTANTTCHILVVAAGALIALFA--FLVSSLVNCFYLLRRLR--NGPRKIYRTCKIQEGSYSSLKQPIREDHFV----- 101
Hu RVB NC 021546 1 MGNRQSSLSQSTHRDINDSHNSNIYLSQASSNEETQCHILVVAAGALIALFA--FLVSSLVNCFYLLRRLR--NGPRKIYRTCKIQEGSYSSLKQPIREDHFV----- 101
Hu RVB AY238391 1 MGNRQSSLSQSTHRDINDSHNSNIYLSQASSNEETQCHILVVAAGALIALFA--FLVSSLVNCFYLLRRLR--NGPRKIYRTCKIQEGSYSSLKQPIREDHFV----- 101
Hu RVB GU391307 1 MGNRQSSAQLNSHLHINSQNSLPISDSKTAVHTCHILVVAAGALIALFA--FLVSSLVNCFYLLRRLR--NGPRKIYRTCKIQEGSYSSLKQPIREDHFV----- 107
Hu RVB JQ904232 1 MGNRQSSAQLNSHLHINSQNSLPISDSKTAVHTCHILVVAAGALIALFA--FLVSSLVNCFYLLRRLR--NGPRKIYRTCKIQEGSYSSLKQPIREDHFV----- 107
Hu RVB GU377230 1 MGNRQSSAQLNSHLHINSQNSLPISDSKTAVHTCHILVVAAGALIALFA--FLVSSLVNCFYLLRRLR--NGPRKIYRTCKIQEGSYSSLKQPIREDHFV----- 107
Hu RVB GU377219 1 MGNRQSSAQLNSHLHINSQNSLPISDSKTAVHTCHILVVAAGALIALFA--FLVSSLVNCFYLLRRLR--NGPRKIYRTCKIQEGSYSSLKQPIREDHFV----- 107
Hu RVB JQ904231 1 MGNRQSSAQLNSHLHINSQNSLPISDSKTAVHTCHILVVAAGALIALFA--FLVSSLVNCFYLLRRLR--NGPRKIYRTCKIQEGSYSSLKQPIREDHFV----- 107
Hu RVB JQ904230 1 MGNRQSSAQLNSHLHINSQNSLPISDSKTAVHTCHILVVAAGALIALFA--FLVSSLVNCFYLLRRLR--NGPRKIYRTCKIQEGSYSSLKQPIREDHFV----- 107
Hu RVB JQ904229 1 MGNRQSSAQLNSHLHINSQNSLPISDSKTAVHTCHILVVAAGALIALFA--FLVSSLVNCFYLLRRLR--NGPRKIYRTCKIQEGSYSSLKQPIREDHFV----- 107
Hu RVB JQ904228 1 MGNRQSSAQLNSHLHINSQNSLPISDSKTAVHTCHILVVAAGALIALFA--FLVSSLVNCFYLLRRLR--NGPRKIYRTCKIQEGSYSSLKQPIREDHFV----- 107
Hu RVB JQ904227 1 MGNRQSSAQLNSHLHINSQNSLPISDSKTAVHTCHILVVAAGALIALFA--FLVSSLVNCFYLLRRLR--NGPRKIYRTCKIQEGSYSSLKQPIREDHFV----- 107
Hu RVB JQ904226 1 MGNRQSSAQLNSHLHINSQNSLPISDSKTAVHTCHILVVAAGALIALFA--FLVSSLVNCFYLLRRLR--NGPRKIYRTCKIQEGSYSSLKQPIREDHFV----- 107
Hu RVB JQ904236 1 MGNRQSSAQLNSHLHINSQNSLPISDSKTAVHTCHILVVAAGALIALFA--FLVSSLVNCFYLLRRLR--NGPRKIYRTCKIQEGSYSSLKQPIREDHFV----- 107
Hu RVB JQ904235 1 MGNRQSSAQLNSHLHINSQNSLPISDSKTAVHTCHILVVAAGALIALFA--FLVSSLVNCFYLLRRLR--NGPRKIYRTCKIQEGSYSSLKQPIREDHFV----- 107
Hu RVB JQ904234 1 MGNRQSSAQLNSHLHINSQNSLPISDSKTAVHTCHILVVAAGALIALFA--FLVSSLVNCFYLLRRLR--NGPRKIYRTCKIQEGSYSSLKQPIREDHFV----- 107
Hu RVB JQ904227 1 MGNRQSSAQLNSHLHINSQNSLPISDSKTAVHTCHILVVAAGALIALFA--FLVSSLVNCFYLLRRLR--NGPRKIYRTCKIQEGSYSSLKQPIREDHFV----- 107
Hu RVB JQ904226 1 MGNRQSSAQLNSHLHINSQNSLPISDSKTAVHTCHILVVAAGALIALFA--FLVSSLVNCFYLLRRLR--NGPRKIYRTCKIQEGSYSSLKQPIREDHFV----- 107
Po RVB KX362373 1 MGNRQSSAQLNSHLHINSQNSLPISDSKTAVHTCHILVVAAGALIALFA--FLVSSLVNCFYLLRRLR--NGPRKIYRTCKIQEGSYSSLKQPIREDHFV----- 115
Ga RVG MF120218 1 MGSNSNVQINQQNHILQASDQSKLNLDQKTTLSLESTQLLGI GAIVVAALII--LIFSLILNCFYLLRRLR--NGPRKIYRTCKIQEGSYSSLKQPIREDHFV----- 106
Ga RVG KY689680 1 MGSNSNVQINQQNHILQASDQSKLNLDQKTTLSLESTQLLGI GAIVVAALII--LIFSLILNCFYLLRRLR--NGPRKIYRTCKIQEGSYSSLKQPIREDHFV----- 106
Ga RVG NC 021583 1 MGSNSNVQINQQNHILQASDQSKLNLDQKTTLSLESTQLLGI GAIVVAALII--LIFSLILNCFYLLRRLR--NGPRKIYRTCKIQEGSYSSLKQPIREDHFV----- 106
Ga RVG JQ920008 1 MGSNSNVQINQQNHILQASDQSKLNLDQKTTLSLESTQLLGI GAIVVAALII--LIFSLILNCFYLLRRLR--NGPRKIYRTCKIQEGSYSSLKQPIREDHFV----- 106
Av RVG MF768259 1 MGSNSNVQINQQNHILQASDQSKLNLDQKTTLSLESTQLLGI GAIVVAALII--LIFSLILNCFYLLRRLR--NGPRKIYRTCKIQEGSYSSLKQPIREDHFV----- 104
Av RVG KC876005 1 MGSNSNVQINQQNHILQASDQSKLNLDQKTTLSLESTQLLGI GAIVVAALII--LIFSLILNCFYLLRRLR--NGPRKIYRTCKIQEGSYSSLKQPIREDHFV----- 104
Ca RVI NC 026820 1 MGSNSNVQINQQNHILQASDQSKLNLDQKTTLSLESTQLLGI GAIVVAALII--LIFSLILNCFYLLRRLR--NGPRKIYRTCKIQEGSYSSLKQPIREDHFV----- 79
Ca RVI KM369898 1 MGSNSNVQINQQNHILQASDQSKLNLDQKTTLSLESTQLLGI GAIVVAALII--LIFSLILNCFYLLRRLR--NGPRKIYRTCKIQEGSYSSLKQPIREDHFV----- 79
Ca RVI KM369887 1 MGSNSNVQINQQNHILQASDQSKLNLDQKTTLSLESTQLLGI GAIVVAALII--LIFSLILNCFYLLRRLR--NGPRKIYRTCKIQEGSYSSLKQPIREDHFV----- 79
Fe RVI KY026790 1 MGSNSNVQINQQNHILQASDQSKLNLDQKTTLSLESTQLLGI GAIVVAALII--LIFSLILNCFYLLRRLR--NGPRKIYRTCKIQEGSYSSLKQPIREDHFV----- 80
```

890

891 **Figure S1.** Alignment of complete RVB, RVG, and RVI NSP1-1 sequences, colored
892 based on amino acid identity, with darker purple indicating higher identity at a given
893 position. RVB Bang117 NSP1-1 is shown in bold text. For each sequence, host origin,
894 rotavirus species, and GenBank accession number are indicated. Av, avian; Ca, canine;
895 Cp, caprine; Fe, feline; Ga, gallinaceous; Hu, human; Po, porcine.

896